PRIMER

Remote epitaxy

Hyunseok Kim[1,2,14], *Celesta S. Chang*[1,2,14], *Sangho Lee*[1,2,14], *Jie Jiang*[3], *Junseok Jeong*[2,4], *Minseong Park*[5], *Yuan Meng*[6], *Jongho Ji*[7], *Yeunwoo Kwon*[7], *Xuechun Sun*[8], *Wei Kong*[8,9]✉, *Hyun S. Kum*[7]✉, *Sang-Hoon Bae*[6,10]✉, *Kyusang Lee*[5,11]✉, *Young Joon Hong*[4,12]✉, *Jian Shi*[3]✉ *and Jeehwan Kim*[1,2,13]✉

Abstract | Remote epitaxy is an emerging technology for producing single-crystalline, free-standing thin films and structures. The method uses 2D van der Waals materials as semi-transparent interlayers that enable epitaxy and release of epitaxial layers at the 2D layer interface. Although the principle of remote epitaxy is simple, it is often challenging to perform owing to stringent requirements for sample preparation and procedure control. This Primer provides extensive guidelines on remote epitaxy techniques, from preparing 2D materials to epitaxy processes and layer transfer methods. Depending on the material of interest, the procedure used can vary, which affects the quality. Consequently, in this Primer, key considerations and characterization techniques are provided for respective families of materials. These are intended as a stepping stone to expand the available material choice and improve the quality of materials grown by remote epitaxy. Lastly, the current limitations, possible solutions and future directions of remote epitaxy and its applications are discussed.

Epitaxial layer
The thin and planar layer of a film formed by an epitaxy process, often abbreviated as epilayer.

Van der Waals (vdW) materials
Materials with strong in-plane atomic bonds but weak out-of-plane vdW interactions.

✉*e-mail:*
kongwei@westlake.edu.cn; *hkum@yonsei.ac.kr*; *sbae22@wustl.edu*; *kl6ut@virginia.edu*; *yjhong@sejong.ac.kr*; *shij4@rpi.edu*; *jeehwan@mit.edu*

https://doi.org/10.1038/s43586-022-00122-w

Epitaxy is a film deposition process where the deposited material has the same crystal orientation as the growth substrate. The crystal surface is generally decorated with dangling bonds from the sudden termination of crystal lattices. This induces periodic fluctuations of electric potential on the surface, which act as the driving force for nucleation of adatoms. Strong chemical bonding occurs at the interface between dangling bonds on the substrate and epitaxially formed materials. As a result, the epitaxial layer bonds tightly to the substrate, with high binding energy. Owing to such tight bonding, it is challenging to physically detach epitaxial layers from their host substrate. However, there is an increasing demand to isolate epitaxial layers for several purposes. Unlike rigid wafers with a thickness of at least several hundred microns, once detached, ultra-thin epitaxial layers can be made lightweight, flexible, bendable and curved. These properties are crucial for emerging applications, including bioelectronics, displays and the internet of things[1,2]. Unprecedented performance and multifunctionality can be achieved by stacking ultra-thin films of different properties and functions, independently grown and exfoliated from different substrates[3,4]. If the substrate is not consumed during the exfoliation process, it can be reused. This is advantageous as substrates are often very costly[5].

Several approaches have been proposed to isolate epitaxial layers from the substrate, such as chemical, mechanical and laser lift-off. Chemical lift-off uses an inserted sacrificial layer between the substrate and the epitaxial layer, which can be dissolved later to obtain a free-standing film[6–8]. The sacrificial layer should have a similar lattice parameter to the substrate and epilayer. A selective etchant is required for the sacrificial layer to minimize damage on the epitaxial film. Controlled spalling, or mechanical lift-off, involves deposition of a stressor layer on the material. This introduces a crack near the edge, which eventually leads to crack propagation parallel to the surface[9,10]. Laser lift-off uses the laser energy absorption difference between materials, such as gallium nitride (GaN) and sapphire (Al_2O_3). A thin region of GaN at the interface absorbs most of the pulsed laser energy and detaches itself from the Al_2O_3 substrate[11]. However, these processes have limitations, including damage to the substrate requiring a refurbishing process, limited choice of materials for selectivity, damage to the interface region of exfoliated layers and low throughput. As a result, their application has been minimal so far.

Recently, remote epitaxy was proposed as a new method for layer transfer and hetero-integration. Using this approach, epitaxy takes place on the substrate coated with thin van der Waals (vdW) materials, typically graphene[12]. Unlike conventional materials formed by strong 3D bondings, in vdW materials, atoms are tightly bound only in in-plane directions by covalent or ionic-type bonding. There is no atomic bonding between each layer in out-of-plane directions, making the layers loosely bound by weak vdW interactions. Therefore, the layered vdW materials can be easily detached in a layer

Author addresses

[1]Department of Mechanical Engineering, Massachusetts Institute of Technology, Cambridge, MA, USA.
[2]Research Laboratory of Electronics, Massachusetts Institute of Technology, Cambridge, MA, USA.
[3]Department of Materials Science and Engineering, Rensselaer Polytechnic Institute, Troy, NY, USA.
[4]Department of Nanotechnology and Advanced Materials Engineering, Sejong University, Seoul, Republic of Korea.
[5]Department of Electrical and Computer Engineering, University of Virginia, Charlottesville, VA, USA.
[6]Department of Mechanical Engineering and Materials Science, Washington University in Saint Louis, St. Louis, MO, USA.
[7]Department of Electrical and Electronic Engineering, Yonsei University, Seoul, Republic of Korea.
[8]Department of Material Science and Engineering, School of Engineering, Westlake University, Hangzhou, Zhejiang Province, China.
[9]Key Laboratory of 3D Micro/Nano Fabrication and Characterization of Zhejiang Province, School of Engineering, Westlake University, Hangzhou, Zhejiang Province, China.
[10]Institute of Materials Science and Engineering, Washington University in Saint Louis, St. Louis, MO, USA.
[11]Department of Material Science and Engineering, University of Virginia, Charlottesville, VA, USA.
[12]GRI–TPC International Research Center, Sejong University, Seoul, Republic of Korea.
[13]Department of Materials Science and Engineering, Massachusetts Institute of Technology, Cambridge, MA, USA.
[14]These authors contributed equally: Hyunseok Kim, Celesta S. Chang, Sangho Lee.

by layer manner owing to their weak binding energy. As a result, there is a pathway to easily isolate atomically thin vdW materials by depositing a handling layer and mechanically detaching it[13,14]. Remote epitaxy combines the advantages of single-crystal, thin film growth from conventional epitaxy with the easy detachability of weak interfaces provided by vdW surfaces. The process is schematically illustrated in FIG. 1.

When a thin graphene layer — such as monolayer or few-layer graphene — is formed on the substrate, either by transfer from foreign templates or by direct growth, the graphene partially screens the electrical and chemical properties of the substrate. If fluctuations in the surface electrostatic potential of the substrate are not completely screened, adatoms on graphene will interact with the substrate lattice. This leads to the formation of epitaxial films with the same crystal orientation as the substrate. In other words, remote interaction between adatoms and the substrate through graphene enables epitaxy despite the graphene interlayer[15,16]. Owing to reduced surface diffusion activation energy on graphene, island nucleation occurs easily on graphene surfaces, which are highly affected by the polarity and ionicity of the underlying substrate[17]. Depending on the growth conditions and time, the nuclei can coalesce to form a smooth film or grow as 3D structures. Because of the absence of direct bonding between graphene and the epitaxial material, the grown film or structure can be readily exfoliated at the graphene interface by mechanical delamination, known as 2D material-based layer transfer (2DLT)[12]. Remote epitaxy and 2DLT methods have enabled a damage-free and high-throughput production of free-standing single-crystal films, which overcome the limitations of existing lift-off processes. Furthermore, remote epitaxy can be applied to virtually any material system as long as the graphene layer does not completely screen the electrostatic potential of the material. However, although remote epitaxy promises a novel and practical path for isolating epitaxial layers from the substrate, technical challenges need to be addressed for practical applications. For example, the interface properties at the 2D interlayer need to be controlled to reliably and reproducibly produce high-quality single-crystal free-standing films by remote epitaxy and 2DLT.

In this Primer, experimental details on implementing remote epitaxy for various materials are explained. Included is a discussion of each step's role and importance and how to characterize the sample. Additionally, the existing and potential applications are introduced, with key considerations for expanding the regime of remote epitaxy.

Experimentation

Remote epitaxy is conducted on substrates covered by atomically thin vdW materials. Consequently, it is critically important to precisely control the formation of vdW layers and their preservation during remote epitaxy. This section introduces the procedures involved in forming the vdW interlayer and graphene; substrates used for epitaxy; suitable conditions and environments; and techniques to isolate remote epitaxial layers from the host substrate by the 2DLT process.

Graphene formation

The template for remote epitaxy is the 2D material-coated crystalline substrate. In general, there are two methods to prepare this; either by first synthesizing the 2D material on a foreign substrate and then transferring it to the growth substrate or by direct synthesis of the 2D layer on the growth substrate. This section focuses on graphene among other 2D materials, as it is the preferred 2D interlayer for remote epitaxy owing to its transparent nature and well-developed processing steps.

In the transfer method, the first step is graphene synthesis. Graphene may be formed either by growth on a catalytic metal surface via chemical vapour deposition (CVD)[18] or by graphitization of hexagonal SiC crystals to form epitaxial graphene on the top surface[19]. The CVD process — where hydrocarbon precursors are decomposed and deposited onto metallic foils such as copper to generate graphene — has been credited for offering an efficient route to produce large-area monolayer graphene using low-cost substrates. However, the graphene formed by CVD is primarily polycrystalline, with micrometre to millimetre-sized domains[18], despite recent progress[20–22]. Pliable and rough copper foil requires a wet transfer process of CVD-graphene onto the target substrate. This process is summarized in Supplementary Fig. 1a. A polymer support — for example, poly(methyl methacrylate) (PMMA) — is spin-coated on graphene. The graphene on the rear side of the copper foil is then etched away by O_2 plasma treatment and the copper foil is removed by dipping in $FeCl_3$ solution. The remaining polymer/graphene stack is rinsed with deionized water and raised out of solution by growth substrates where remote epitaxy will be conducted. Finally, the polymer support is removed by

Electrostatic potential
The amount of work needed to move an electric charge.

2D material-based layer transfer
Exfoliation and transfer of layers at the interface formed by 2D materials.

Wet transfer process
Transfer of 2D materials onto a target substrate in liquid.

dissolving it in an appropriate solvent, such as acetone for PMMA. However, this wet transfer method is likely to introduce a significant amount of unwanted defects, including wrinkles, holes, polymer residues and interfacial contamination, which could disturb remote interaction between the substrate and the epitaxial film through graphene. Therefore, the wet transfer method can only be used for remote epitaxy of certain materials, which will be discussed in detail in the later sections.

Alternatively, epitaxial graphene can be produced by sublimating the top silicon face and rearranging the remaining carbon atoms on single-crystalline SiC wafers[19]. As-grown SiC-graphene is single-crystalline over the whole SiC surface. A dry transfer process can be used, aided by the stiff and atomically flat SiC wafer (see Supplementary Fig. 1b). In the dry transfer method, nickel is first deposited on graphene as a stressor layer. The initial deposition of nickel needs to be conducted by electron-beam evaporation or thermal evaporation to prevent damage to the graphene lattice by ion bombardments during sputtering. Once the graphene is fully covered by evaporated nickel, sputtered nickel can be used for further deposition. Next, thermal release tape (TRT) is applied on the nickel/graphene/SiC substrate to mechanically exfoliate the nickel/graphene stack from the SiC substrate. The released TRT/nickel/graphene stack is then manually attached to the growth substrate, where graphene forms vdW bonding with the substrate. The TRT can then be removed at an elevated temperature, such as 80–150 °C, on hot plates. Lastly, nickel is removed by dipping the sample in a nickel etchant, followed by water rinsing and blow-drying. The type of nickel etchant needs to be chosen based on the reactivity of the etchant with the substrate material to ensure the substrate is not damaged during the nickel etching process. The dry transfer process can be conducted in air for the materials introduced in the primer. Compared with the wet transfer process of graphene from copper foils, dry transfer of SiC-graphene is less likely to introduce wrinkles and residues in graphene, leading to high-quality graphene uniformly covering the substrate. Also, as no water or any other liquid can be trapped between the graphene and the substrate, dry transfer ensures a much cleaner interface. However, the major downsides of this approach are the high cost of SiC wafers and the process for graphitization, which requires extremely high temperatures around 1,500 °C.

An alternative method of forming graphene is its direct growth on the substrate that can be used directly for remote epitaxy. Unlike epitaxial graphene, which can only be grown on SiC wafers, CVD-graphene can be synthesized on metal, semiconductor and insulator substrates, which are of vital importance for advanced electronic/photonic applications. For example, it has been reported that monolayer graphene can be grown on germanium[23], Al_2O_3 (REFS[24,25]), SiO_2 on silicon (REF.[26]) and glass substrates[27]. However, owing to its high growth temperature — typically above 900 °C — it is difficult to grow high-quality graphene directly on substrates that cannot sustain such high temperatures. Recently, reports on low-temperature growth of sp^2-bonded 2D materials, such as amorphous carbon[28] and amorphous boron nitrides[29], have suggested that there is potential to use them as remote epitaxial templates directly formed on thermally weak substrates. By direct formation of

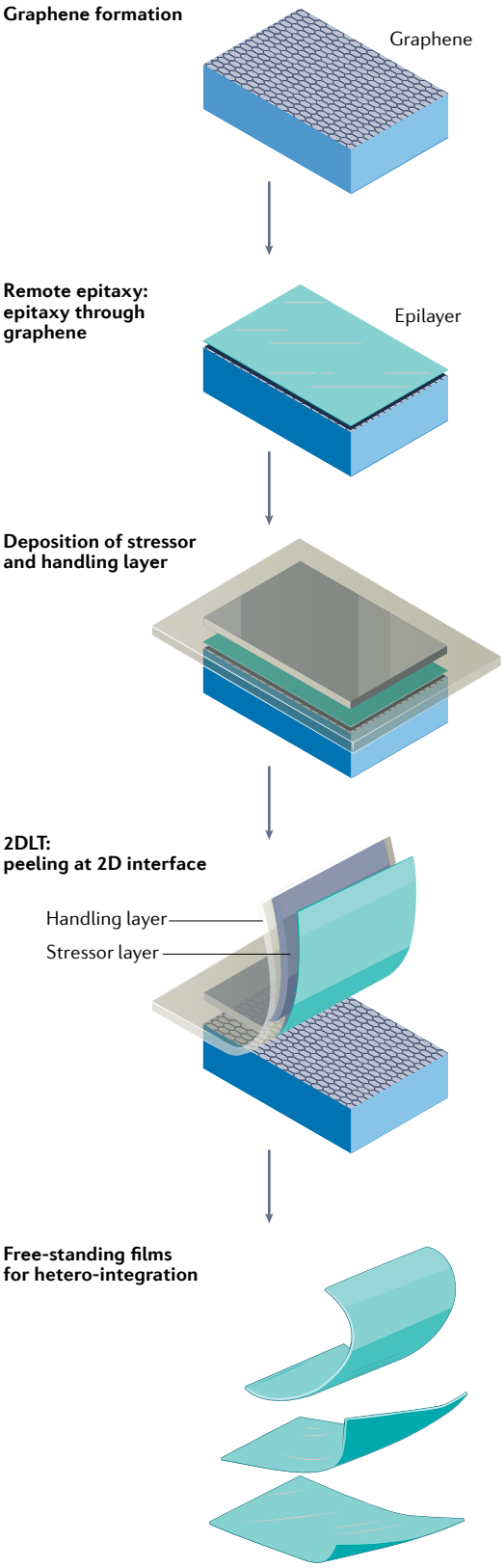

Fig. 1 | **Remote epitaxy and layer transfer process.** 2DLT, 2D material-based layer transfer.

Dry transfer process
Transfer of 2D materials onto a target substrate without liquid at the interface between the 2D material and the substrate.

Direct growth
The formation of materials directly on the target substrate instead of forming them elsewhere and then transferring them onto the target substrate.

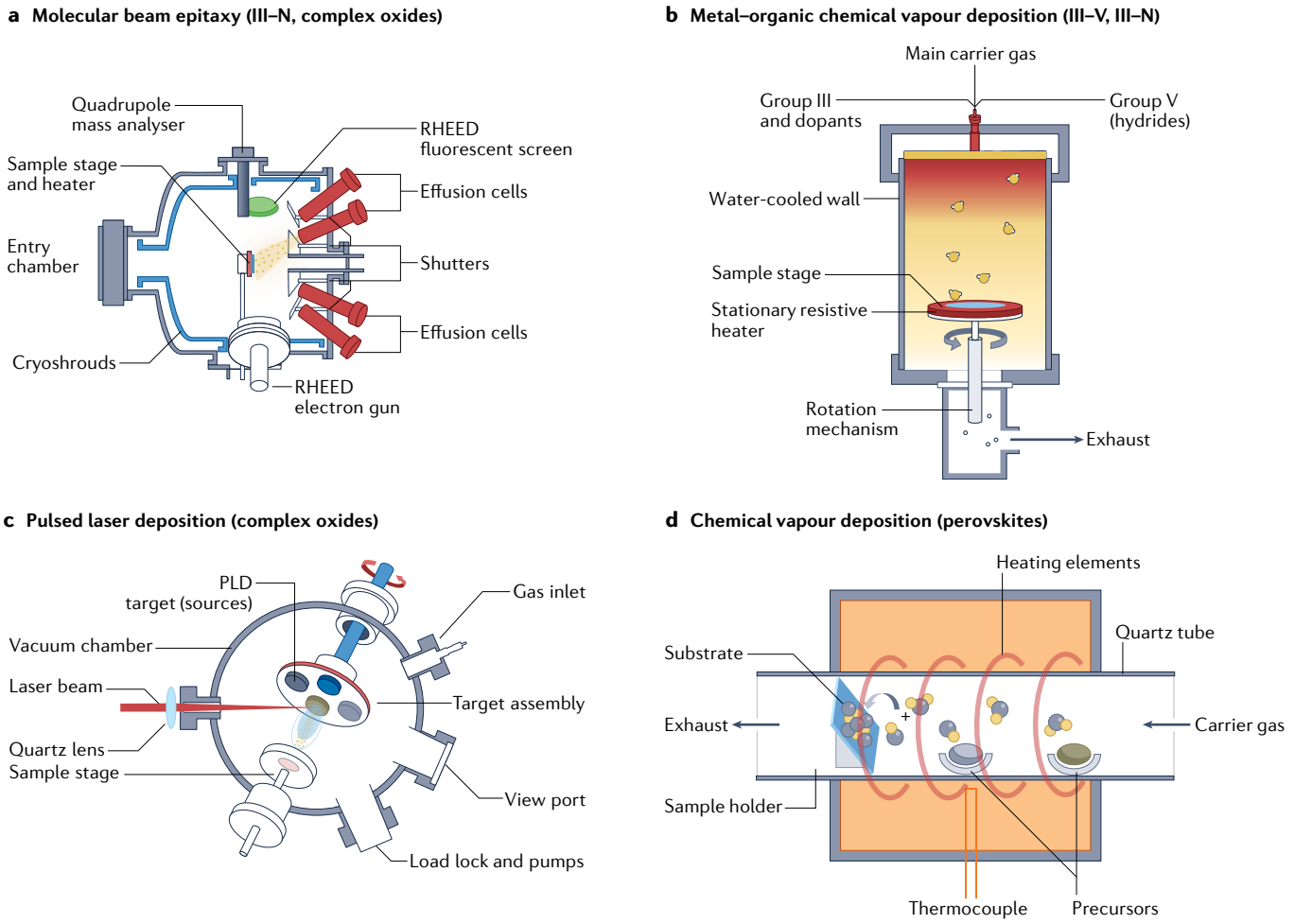

Fig. 2 | **Equipment for remote epitaxy. a** | Molecular beam epitaxy (MBE). **b** | Metal–organic chemical vapour deposition (MOCVD). **c** | Pulsed laser deposition (PLD). **d** | Chemical vapour deposition (CVD). RHEED, reflection high-energy electron diffraction. Part **a** adapted with permission from REF.[137], Elsevier. Part **b** adapted with permission from REF.[138], AIP. Part **c** adapted from REF.[139], Springer Nature Limited. Parts **a**–**c** adapted from REF.[1], Springer Nature Limited.

graphene, the graphene surface and the interface can be made free of process residues and defects, which is an ideal template for remote epitaxy with the cleanest interfaces. The process will also become highly scalable, making this approach fascinating for remote epitaxy and related applications.

Once graphene is formed on the substrate, remote epitaxy can be conducted using several epitaxy tools. Widely used systems for remote epitaxy are summarized in FIG. 2, although other epitaxy tools can also be employed.

Material growth by remote epitaxy

III–V (III–As and III–P). GaAs was the first material on which remote epitaxy was demonstrated[12]. However, it was later realized that III–V compound semiconductors such as GaAs have relatively weak interaction through graphene, imposing stringent requirements to attain single-crystal growth by remote epitaxy[30,31]. This is because the ionicity of materials strongly affects the electrostatic potential fluctuation on their surface. GaAs is a partially ionic material with relatively low ionicity[32], and the surface electrostatic potential fluctuation quickly diminishes as the distance from the surface increases. Density functional theory calculations reveal that remote epitaxy of GaAs will not work if graphene is thicker than a monolayer[15]. Consequently, remote epitaxy of III–V compound semiconductors — including GaAs, InP and GaP — have only been reported on substrates covered with monolayer graphene[12].

The weak interaction through graphene also implies that the interface properties are critically important for successful remote epitaxy. Residue above or below the graphene layer, or oxidation of the substrate, can increase the effective distance between the partially ionic substrate and the adatoms above graphene. As a result, the remote interaction may be completely screened, leading to the formation of polycrystalline domains. Therefore, it is crucially important to preserve pristine surfaces in remote epitaxy of III–V materials, which is difficult when the conventional wet transfer process is used to prepare the graphene. During wet transfer of graphene from copper foils onto III–V, graphene is raised by III–V substrates in water and then dried. If water is trapped at the interface between the graphene and the substrate, it can induce the formation of native oxides during the drying process. The interfacial formation of native oxides

III–V compound semiconductors
Compound semiconductors composed of group III (such as aluminium, gallium, indium) and group V (such as arsenic, phosphorus, antimony), typically forming zinc-blende crystal structures.

prevents single-crystal growth of remote epitaxial III–V thin films, which can be observed by X-ray photoelectron spectroscopy (XPS)[30]. Therefore, the graphene needs to be transferred onto III–V substrates by dry transfer immediately after deoxidation of III–V substrates by wet etching, water rinsing and blow-drying. This ensures a pristine graphene–substrate interface without native oxides, which provides a viable path for remote epitaxy of III–V[12,30,31]. However, any graphene transfer process inevitably induces damage on graphene, such as tearing, folding and contamination, which affects the quality of remote epitaxial films and the capability to isolate the film at the interface. Directly grown 2D materials on III–V substrates that do not require a transfer process would be an ideal pathway for future remote epitaxy. The growth of 2D materials on III–V substrates is in the early stage of development.

After graphene formation on III–V substrates, remote epitaxy of III–V can be achieved using any III–V epitaxy tools, such as metal–organic chemical vapour deposition (MOCVD), molecular beam epitaxy (MBE) and hydride vapour phase epitaxy (HVPE). Currently, experimental demonstration has only been reported with MOCVD. The growth of GaAs thin films by remote epitaxy can be achieved under a standard GaAs epitaxy condition. Adding a low-temperature nucleation stage can enhance the density of nuclei and promote quick planarization of the film[12,30]. Because epitaxy of III–V takes place at a high temperature, it is critically important that neither the graphene nor the substrate is damaged under the harsh epitaxy environment. For example, under an MOCVD growth environment, hydrogen carriers can damage graphene and prevent remote epitaxy, necessitating a nitrogen carrier for remote epitaxy[30]. This principle may also apply for HVPE, where radicals from hydride sources in the HVPE interact with graphene, meaning that the growth conditions and parameters need to be carefully studied. In this regard, MBE can ensure the most pristine environment optimal for remote epitaxy because the growth is conducted with elemental sources in ultra-high vacuum conditions at a relatively low temperature. If native oxides form on the surface, they can dissociate at high growth temperatures and damage the graphene. This emphasizes the importance of obtaining pristine interfaces during the transfer process. In summary, the remote epitaxy of III–V requires stringent control in preparing graphene-coated substrates and growing remote epitaxial films owing to the sensitivity of remote interaction at the atomic scale.

III–N. Remote epitaxy of III–N can be achieved using MBE or MOCVD[15,33–36]. After thorough degreasing and native oxide removal of the crystalline substrate with hydrochloric acid[37], graphene is transferred onto growth substrates by either wet or dry transfer. After outgassing to remove the surface absorbates on the graphene-coated substrate, remote epitaxial growth is initiated using typical growth methods for III–N in MBE or MOCVD, respectively[37–39].

The remote epitaxy of III–N operates under relatively weak dipole interactions. As a result, factors such as the choice of substrate, 2D material, transfer method and growth conditions can alter or disrupt the process. In general, remote epitaxy of III–N does not require exact matching of crystalline lattices between the remote epitaxial layer and the substrate. For example, III–N can be remote epitaxially grown on graphene-coated GaN, AlN, Al_2O_3 and SiC[15,33,35,40–42], which have the same or a relatively similar hexagonal lattice arrangement to III–N. In general, the crystal quality of remote epitaxial films decreases when the substrate is not lattice-matched, and the crystal quality of the substrate affects the quality of grown films[43]. Graphene of different origins — including polycrystalline CVD-graphene and single-crystalline epitaxial graphene — have been used as the interlayer for III–N remote epitaxy[33,35,42,43]. Reports show that defects in graphene, intentional or unintentional, can disrupt the nucleation induced by remote interaction with the substrate, altering the growth mechanisms and crystal quality[30]. Wet-transferred graphene involves a polymer, and contamination caused by polymer residues can disturb the remote epitaxy. Consequently, the dry transfer process is preferred to attain high-quality remote epitaxial films[44]. Although III–N is a compound semiconductor with relatively strong ionic bonds, the graphene spacer should be kept below three layers owing to the fast attenuation of dipole interactions away from the substrate beneath the graphene[15]. Therefore, remote epitaxy of GaN on epitaxial graphene formed on a graphitized SiC substrate, which does not require transfer processes, is a promising method to produce high-quality GaN films. This is particularly useful as there is the capability to repeatedly reuse the SiC substrate[33]. When the thickness of epitaxial graphene is reduced, III–N's nucleation density and crystal quality can be improved[33]. Al_2O_3 substrates coated with CVD-grown graphene are also an effective template for remote epitaxy of III–N that does not require graphene transfer[35,36]. Although graphene is the most suitable interlayer, various 2D materials may be used instead, including hexagonal boron nitride (h-BN) and transition metal dichalcogenides (TMDCs). However, the polar nature of the h-BN and TMDCs can interfere or screen interactions from the substrate, disrupting remote epitaxy[15]. Finally, damage to 2D materials should be avoided, because the growth of III–N materials typically involves harsh conditions, such as reactive precursors and high temperatures. In conventional III–N epitaxy, the optimal growth conditions are typically at or around the dissociation point of III–N, which involves constant surface reconfiguring. For remote epitaxy of III–N, however, intense surface dynamics leading to the dissociation of III–N surfaces is thought to be responsible for damage of 2D interlayers[45]. As a result, although no consensus has been reached on the best growth procedure and conditions, a two-step method is preferred for III–N remote epitaxy. The first step should use a lower temperature, with a gentle flux of precursors until the grown film fully encapsulates 2D interlayers, followed by a second step at a higher temperature for high-quality film growth[46].

Complex oxides. Complex-oxide materials can be epitaxially grown using two techniques. The first technique, called pulsed laser deposition (PLD), ablates a

III–N
A special form of III–V compound semiconductors with nitrogen as a group V element, typically forming wurtzite crystal structures.

Pulsed laser deposition
An epitaxial growth technique that uses short pulses of high-intensity lasers to ablate a polycrystalline target material onto a single-crystalline substrate.

polycrystalline source material using a high-energy excimer laser (KrF, 248 nm). When the laser strikes the source material, the material is vaporized and deposited onto the substrate. The substrate is heated in a way that enables atoms reaching the surface to align epitaxially with the substrate. Another technique uses oxide MBE. The MBE equipment allows the flow of oxygen during growth. It is imperative that O_2 is used as the oxygen source when the graphene is exposed (usually during the nucleation stage) instead of ozone, as ozone will instantly etch the graphene. Owing to the energetic PLD growth process, the graphene may be damaged during the initial nucleation of the epitaxial film, which can be prevented by transferring double layers of graphene and reducing oxygen flow during the first few monolayers of growth[3]. This is not an issue for MBE growth owing to its soft growth process.

Remote epitaxy of complex-oxide thin films starts with the transfer of graphene onto a single-crystalline, complex-oxide substrate[3]. It is important that the sample surface is prepared in the same manner as conventional epitaxy. For example, for the growth of strontium titanate ($SrTiO_3$, abbreviated as STO), an archetypal perovskite material, the surface must be TiO_2 terminated. This can be achieved by immersing it in hydrofluoric acid and annealing at high temperatures[47]. Afterwards, the graphene can be dry-transferred onto the STO surface. A similar process is used for other complex-oxide substrates, such as magnesium aluminate ($MgAl_2O_4$ or MAO) and gadolinium gallium garnet ($Gd_3Ga_5O_{12}$, typically abbreviated as GGG).

The type of graphene used is the most important variable for allowing high-yield exfoliation of remote epitaxially grown complex oxides via PLD. A single-crystal graphene layer grown on SiC substrates must be used. Polycrystalline CVD-grown graphene cannot withstand the harsh plasma environment of the PLD during the nucleation stage, leading to exfoliation failure. For the transfer of epitaxial graphene grown on SiC substrates, dry transfer processes with a nickel handling layer need to be used. After transferring the tape/nickel/graphene/substrate stack and removing the tape on a hotplate, the stack is immersed in a solution of $FeCl_3$. The stack is left in the solution until the nickel is completely etched. Gentle stirring is necessary before pulling out the graphene/complex-oxide substrate to prevent nickel redeposition. The graphene/complex oxide is then rinsed in deionized water for 15 min until the $FeCl_3$ is completely removed. The graphene/complex-oxide substrate must be handled carefully to prevent delamination of graphene from the substrate surface. The final step is to rinse the sample in acetone and isopropyl alcohol (IPA) for 1 min each to remove any remaining water on the surface.

Finally, the graphene/complex-oxide stack is placed inside the epitaxial growth chamber, and the growth is performed as usual. It is worth noting that the growth condition may require some changes because initial nucleation may be reduced from growth on graphene surfaces compared with normal substrate surfaces[48].

Halide perovskites. To develop high-performance halide perovskite-based optoelectronic devices, synthesis of uniform and grain boundary-free perovskite films is essential[49–52]. Vapour and solution phase epitaxy methods were developed to grow high-quality, thickness-controlled halide perovskite films with low-density defects[53–57]. One practical challenge for most vapour phase epitaxy approaches is that the epitaxial films cannot be readily used for device fabrication because the epitaxial substrates are often electronically inactive. Additionally, the use of lattice-mismatched substrates often leads to the creation of optoelectronically harmful dislocations, impacting the performance of devices. Remote epitaxy of halide perovskites was developed to address these issues[48].

Alkali halides are the preferred universal substrates for ionic epitaxy of halide perovskite films because they have a similar lattice constant and material chemistry to halide perovskites[56,58]. As alkali halides are water-soluble, the preparation of graphene-coated alkali halide substrate is slightly different to the typical wet transfer process[48]. The process first follows the standard wet transfer process, such as spin-coating PMMA on graphene/copper foil and etching graphene on the rear side of copper by O_2 plasma. After this, the PMMA-coated graphene/copper is immersed in an ammonium persulfate (APS) aqueous solution (60 g l^{-1}) to etch copper away. After etching, the PMMA-coated graphene is rinsed in IPA several times, and the floating film is gently lifted using an alkali halide substrate, for example NaCl. Finally, after drying in air, the PMMA is dissolved in acetone, and the graphene-coated alkali halide substrate is developed. CVD has been used for remote epitaxy of halide perovskite films. The graphene-coated substrate is placed in the low-temperature and downstream region of the CVD chamber, whereas CsBr and $PbBr_3$ in powder form are placed in the upstream regions for growth of $CsPbBr_3$. These positions should be optimized to obtain suitable vapour pressures of precursors and supersaturation on the substrate. Argon gas flow is introduced to transport the precursors onto the substrate before a remote epitaxial layer is grown with the centre of the CVD tube typically kept at 500 °C.

Microstructures and nanostructures. Non-planar remote epitaxial microstructures and nanostructures with various shapes — including rods, discs, wires and needles — have been grown on graphene-coated wafers via hydrothermal[59–61] and MOCVD[16,41] techniques. So far, the graphene interlayer on ZnO, GaN and Al_2O_3 substrates has been prepared by wet-transferring CVD-grown polycrystalline graphene on copper foils; however, dry transfer processes can also be used. After wet transfer of graphene onto a single-crystalline wafer of interest, the substrate is annealed at hydrogen ambiance. The graphene layer should be thin enough so that the graphene layer does not completely screen the substrate. In the meantime, it is advised to make the graphene thick enough to avoid direct covalent epitaxy through pinhole-like defects and unwanted torn apertures of graphene[15,59]. Typically, hydrothermal remote epitaxy of ZnO on ZnO and GaN substrates requires interlayer thickness of one to three layers of graphene[59,60], and MOCVD-based remote epitaxy of GaN on c-Al_2O_3 requires one or two layers of graphene[16]. If the graphene

is defective, a fraction of the grown structures cannot be exfoliated by the 2DLT process. Instead, they remain on the substrate because of a direct covalent epitaxy through the defective region[41]. Therefore, a pinhole-free graphene layer is crucial for the successful exfoliation of microstructures and nanostructures. This may be achieved by transferring graphene twice onto the substrate so that the other layer of graphene covers pinholes in each layer.

For the hydrothermal remote epitaxy of ZnO micro-rods, a-ZnO and c-ZnO substrates are formed as films on r-Al_2O_3 and c-GaN wafers, respectively. Then, the two substrates are dipped in an equimolar (25.0 mM) nutrient solution of zinc nitrate hexahydrate ($Zn(NO_3)_2{\cdot}6H_2O$) and hexamethylenetetramine ($C_6H_{12}N_4$) dissolved in deionized water at 95 °C for 4 h in a Teflon-lined autoclave for hydrothermal synthesis[59]. Hydrothermal synthesis can be applied to control the morphology of ZnO microstructures into submicron wires, rods, discs, needles and more, depending on the chemicals and additives of the nutrient solution[61]. Hydrothermal remote epitaxy of ZnO is possible across up to three graphene layers on both substrates.

Meanwhile, MOCVD can be used for remote epitaxy of GaN hexagonal micro-rods on c-Al_2O_3. The low-temperature buffer layer typically applied in GaN thin film epitaxy on Al_2O_3 is not adopted in this case. The flow rate of ammonia (NH_3) is decreased by two orders of magnitude from typical thin film growth conditions. The high nucleation temperature decreases the nucleation density, whereas the high III/V flow rate ratio enables unidirectionally elongated wire-shaped crystal growth[62,63]. As a result, spatially isolated microstructures and nanostructures form. The remote epitaxy has a 30°-rotated in-plane relation to minimize the large lattice mismatch strain — a = 3.186 Å and a = 4.785 Å for GaN and Al_2O_3, respectively — similar to covalent epitaxy of GaN on Al_2O_3 (REF.[16]). In MOCVD, trimethylgallium (TMGa) and NH_3 are used for gallium and nitrogen precursors. A high TMGa to NH_3 molar flow ratio is used to form rod-shaped microstructures as an n-type core. The temperature and flow rate profiles of typical thin film InGaN quantum wells and p-type GaN are adopted on n-type core micro-rods to form multi-quantum well heterostructures that can be used to fabricate light-emitting diodes (LEDs). The facet direction of microstructures is found to be homogeneous over the whole surface of the graphene-coated wafer, regardless of the growth methods and domain size of graphene. This indicates that the potential field penetrated across graphene is strongly driven by the underlying wafer rather than the vdW interaction with graphene[60].

In addition to hexagonal rods, remote epitaxy of GaN tetrahedron microstructures can be grown on graphitized SiC substrates using MOCVD[40]. The microstructures formed on graphene exhibit a perfect geometrical tetrahedron shape which reflects the high crystallinity achieved by strain relaxation of GaN crystals on graphene. By flowing NH_3 during the annealing step before growth, all tetrahedron microstructures are aligned to have the same in-plane orientation with the substrate, meaning that GaN crystals are remote epitaxially grown.

The methods discussed have no control over the position of microstructures. By contrast, selective-area remote epitaxy can precisely control the crystal position by preparing a patterned mask layer on the graphene-coated wafers. A hydrophobic surface is required as the mask layer. This prevents nucleation–growth of overlayer materials during hydrothermal remote epitaxy of microstructures. The graphitic layer, whose thickness is at least four graphene layers, can be used as a growth mask where the growth is inhibited. In other words, the thickness of graphene on the growth sites should be reduced for remote epitaxy, which can be achieved by standard electron beam or photolithographic patterning procedures[64,65].

Layer transfer by the 2DLT process

2DLT generally involves remote epitaxy[15,30,48,66] or vdW epitaxy[34,67,68] to grow single-crystalline thin films on top of 2D materials, which can be mechanically exfoliated from the host substrate to produce high-quality free-standing thin films for heterogeneously integrated and physically coupled devices and applications. Conventional layer transfer methods — chemical lift-off, laser lift-off or mechanical spalling — are either time-consuming for wafer-scale release, damaging to the interface or challenging to control the spalled depth for producing smooth samples[9]. By contrast, 2DLT can be an efficient mechanical exfoliation process with high throughput and clean interfaces. More importantly, the spalling depth can be precisely controlled by the position of the interfacial 2D layer with atomic precision[22,69,70]. As no covalent bindings are, in principle, formed between the substrate and the epilayer, it enables efficient host wafer recycling without the need for a refurbishing process[3,71].

Once grown, the thin films or microstructures/nanostructures can be exfoliated at the interface by 2DLT, as schematically shown in FIG. 1. The 2DLT process for thin films can be achieved by deposition of a stressor layer, followed by deposition or attachment of a handling layer[1]. Sputtered nickel is widely used as a stressor layer, where the tensile stress facilitates the exfoliation of remote epitaxial films at the interface[14]. However, other materials may be used instead. Typically, a thin layer of nickel (less than a few micrometres) with a low stress level is sufficient for the exfoliation, but in some cases metal stressors are unnecessary[71]. Another role of the metal stressor is supporting the film, because it can crack during exfoliation, especially if the film is severely curved. A thin adhesion layer, such as titanium or chromium, can be deposited on the remote epitaxial films before sputtering for enhanced adhesion strength. TRT is often applied for handling layers because it can be easily removed. Other handling materials, such as polydimethylsiloxane (PDMS), can be leveraged depending on the fabrication processes[3,12,71]. After the stressor and handling layers are formed, the stack is peeled off from the edge of the samples or wafers by mechanical exfoliation. The exfoliated film can then be transferred and attached to any substrate of interest by mechanically pressing the stack, releasing the tape and etching away the metal layer.

The 2DLT processes for microstructures and nanostructures are slightly different because merged films are not formed by remote epitaxy. As a result, gaps between these structures need to be filled by a polymeric layer to support them (see Supplementary Fig. 2). Spin-coated polyimide (PI) is suitable for fabricating flexible devices because PI is electrically insulative, mechanically deformable, thermally tolerant up to 400 °C and easily removable by oxygen plasma treatment[72–74]. Stressor layers are typically not required for the exfoliation of microstructures and nanostructures.

After the exfoliation of remote epitaxial films or microstructures/nanostructures, residues from the metal or handling layer need to be carefully cleaned for device fabrication. Also, because graphene has weak adhesion to the substrate, the graphene layer can partially be exfoliated with the film. Therefore, depending on the applications, the exfoliated graphene, which partially covers the exfoliated film's interface side, needs to be removed. Because the 2DLT technique can enable heterogeneous integration of dissimilar materials with clean 2D/3D and 3D/3D interfaces, this technique provides a powerful and flexible tool to produce diverse categories of high-quality and functional devices when combined with remote epitaxy.

Results

This section looks at a few representative characterization techniques for remote epitaxy. First, characterization methods for 2D material-coated substrates are introduced. Next, techniques are explained for characterizing the crystal quality and topography of remote epitaxially grown films and microstructures/nanostructures. Lastly, this section shows how the exfoliation results of remote epitaxial layers can be assessed.

Graphene characterization

Proper characterization of the graphene-coated surface is needed to identify the crystallinity, cleanliness and morphology of the as-prepared remote epitaxial template. This process is essential for technique success and troubleshooting in the case of failure. The most important information is determining the number of graphene layers and their quality. If graphene is damaged during any process, epitaxy can take place through pinholes formed in the graphene layer followed by lateral overgrowth[75–77].

Mixed growth modes of remote epitaxy and pinhole-seeded lateral overgrowth complicate the study and damage the substrate during the 2DLT process. Rigorous characterization of graphene is necessary for both material investigation and device applications. For non-destructive characterization of graphene, Raman spectroscopy[78], XPS[79], atomic force microscopy (AFM)[80] and scanning electron microscopy (SEM)[81] are widely used.

Raman spectroscopy is relatively simple to perform in terms of the experiment set-up and time required. The experiment is typically performed by exciting the sample with a visible laser and measuring the Raman scattering at the Raman shift range of graphene-related peaks, such as the D peak (~1,350 cm^{-1}), G peak (~1,580 cm^{-1}) and 2D peak (~2,700 cm^{-1})[82]. The quality and thickness of graphene can be deduced from the peak positions, linewidth and relative intensities, making Raman spectroscopy one of the most effective tools to characterize graphene properties[78]. For example, the presence of a D peak indicates a defective nature of graphene (FIG. 3b), and the position and linewidth of the 2D peak indicate the thickness of graphene[82] (as shown in the spectra in FIG. 3a). In the case where Raman peaks of graphene overlap with the substrate peak — for example, as-grown graphene on SiC where the SiC second-order Raman peaks between 1,450 and 1,750 cm^{-1} are superimposed on the G peak of graphene — the Raman spectrum of bare SiC needs to be subtracted from the total spectrum. XPS is also often used to characterize the quality of graphene. The *D* parameter, extracted from the carbon KLL Auger transition, is measured to differentiate between the sp^3 and sp^2 character of carbon bonds, where the sp^3-bonded portion indicates lattice defects in graphene[79]. The *D* parameter increases from monolayer to multilayered graphene as the thickness of graphene contributing to the carbon KLL signal increases. X-ray reflectivity can also be used to estimate graphene thickness. The carbon 1*s* spectra at 285 eV are normally used as a reference for the peak fitting analysis. Although these methods require fitting and further analysis of the spectrum to extract the number of graphene layers, AFM can directly measure the thickness and damage in graphene[80,83]. From AFM, the height of graphene can be measured at the edge of the graphene layer as shown in FIG. 3c–e. AFM can also probe residue or holes in graphene. Additionally, SEM can be used to confirm the coverage of graphene[81]. Under SEM, graphene-coated regions exhibit contrast differences from clean surfaces without graphene. Although it is hard to tell the thickness directly, SEM can identify multilayer graphene regions such as bilayer stripes or thick graphene islands. Besides these methods, other techniques, such as transmission electron microscopy (TEM)[84] and scanning tunnelling microscopy[85], may also be employed to characterize graphene's structural and chemical properties.

Film and structure characterization

A list of reported remote epitaxial films and structures is given in TABLE 1. The quality of remote epitaxial films can be predetermined from in situ reflection high-energy electron diffraction (RHEED), which monitors the surface structure during growth. RHEED uses a high-energy (10–30 keV) electron beam to record the reflected beam from the growth surface. The period of the intensity oscillations corresponds to one monolayer of growth[86]. Before the growth initiation, RHEED patterns can reveal the presence or desorption of native oxides. Once the growth is initiated, a 2D layer by layer growth mode would lead to a smooth single-crystalline growth, resulting in elongated spectral spots, referred to as streaky spots. If a transition occurs from 2D to 3D island growth, the electron beam will pass through the island, creating a spotty pattern similar to an electron diffraction pattern from the bulk material. This can be a useful signature to detect the growth of polycrystalline films. After the growth is finished and the sample is taken out of the epitaxy tool,

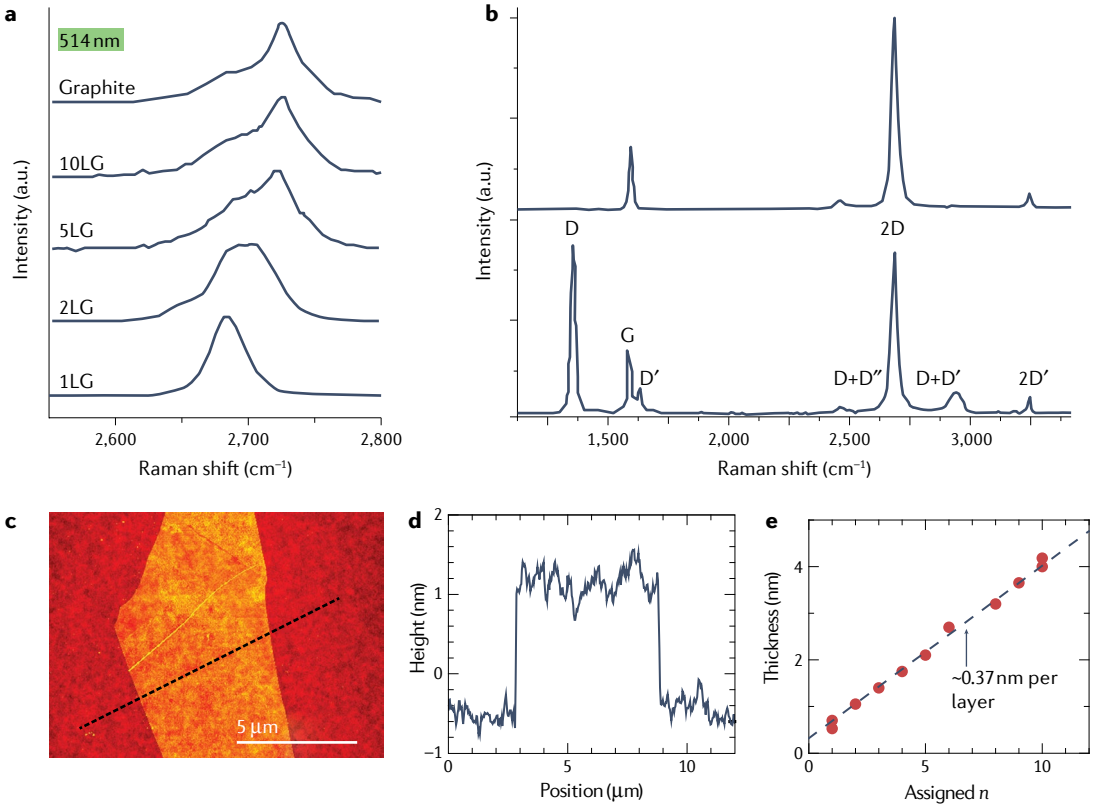

Fig. 3 | **Characterization of graphene. a** | Raman spectra of 2D peak as a function of graphene thickness. **b** | Representative Raman spectra of pristine (upper) and defective (lower) monolayer graphene. **c** | Atomic force microscopy (AFM) image of four-layer graphene. **d** | Height profile along dashed line in panel **c**. Graphene thickness can be determined from average step heights at edges of graphene layers. **e** | Thickness measured by AFM of selected graphene flakes. Dashed line fits to thickness measurements. All Raman spectra and AFM images are measured on graphene transferred onto SiO_2 on silicon substrates. 1LG–10LG, monolayer graphene–10-layer graphene. Part **a** adapted with permission from REF.[140], APS. Part **b** adapted from REF.[82], Springer Nature Limited. Parts **c**–**e** adapted with permission from REF.[83], ACS.

the crystallinity of the epilayer can be measured by X-ray diffraction (XRD). From the 2θ–ω and φ-scans of XRD, where ω, 2θ and φ correspond to the beam incident angle, diffracted angle and rotation of the sample, respectively, the out-of-plane and in-plane orientation of the film can be revealed. Rocking curve (ω-scan) measurements provide information on the quality and thickness of the film, whereas reciprocal space maps can determine the strain properties[87]. Using SEM, the surface morphology of the epitaxial layer can be observed with sufficiently high magnification to examine the textured or smooth surface[88]. Observing the morphology of textured surfaces can support the XRD identification of different domains or phases, as they tend to grow along a particular orientation or have a distinguishable crystallinity to create a rough surface. Electron backscatter diffraction (EBSD) is an SEM-based technique that can visually map the 3D orientation of the crystal lattice and phase information at each data collection point[89]. All of the above characterization methods discussed are non-destructive methods, ensuring safe data collection without damaging the epitaxial layer.

The quality of the epitaxial layer at an atomic scale can be examined by extracting cross-sectional specimens using a focused ion beam[90]. The sample is protected from damage by the ion beam by depositing carbon (fifty to hundreds of nanometres thick) and platinum layers (~1 µm thick) on the region of interest in the SEM focused ion beam chamber. Trench milling is undertaken at a voltage of 30 kV, using an initial current at 9.5 nA and finishing with 2.5 nA. Once mounted on a TEM grid, sample thinning is performed at 30 kV, 80 pA. Final sample milling occurs at 5 kV, 68 pA to minimize redeposition. For sensitive samples, 2 kV, 89 pA is often used at the final stage. Once the specimen is prepared, it can be plasma-cleaned using an argon and nitrogen gas mixture for 30–180 s when loaded onto the TEM sample holder. However, avoiding plasma cleaning is suggested as it can damage the graphene, especially when the sample thickness is thin (<30 nm). Scanning transmission electron microscopy (STEM) can be used on the sample at various voltages (60–300 kV) to obtain information on crystallinity, domains, defects, dislocations or chemical composition of the film[91]. Higher beam voltages produce robust atomic lattice images for the epitaxial film grown on graphene, although the graphene is easily damaged when imaging at a small field of view. As a result, the beam voltage and current — the electron beam dose — should be carefully selected. Depending on the detector geometry, high-angle annular dark-field (HAADF) STEM produces images with a contrast roughly proportional to $Z^{1.7}$, where Z is the atomic number[92].

If the epitaxial layer is composed of heavy elements, the graphene layer consisting of light carbon atoms will not be visible. In this case, annular bright-field STEM images can be simultaneously acquired to create an image with a less stark contrast between elements, making graphene more visible[93]. From atomic-resolution STEM imaging, types of defects and dislocations can be identified. Using energy dispersive spectroscopy or electron energy loss

Table 1 | **Reported materials and processes for remote epitaxy**

Grown layer	Substrate material	2D interlayer material	Interlayer formation	Growth method	Note	Refs
GaAs	GaAs	Monolayer graphene	Dry transfer	MOCVD	Transfer method significantly affects the quality of remote epitaxy	12,15,30,31
InP	InP	Monolayer graphene	Dry transfer	MOCVD	N_2 carrier is used for growth	12
GaP	GaP	Monolayer graphene	Dry transfer	MOCVD	N_2 carrier is used for growth	12
(In)GaP	GaAs	Monolayer graphene	Dry transfer	MOCVD	Graphene allows for spontaneous relaxation of epilayer	95
GaN	GaN, Al_2O_3	One or two-layer graphene	Dry transfer, wet transfer	MOCVD, MBE	Single-crystal growth up to two graphene layers	15,128–130
GaN	SiC	Monolayer graphene	Grown	MBE, MOCVD	Both epitaxial graphene and graphene buffer layer can be used	33,34
AlN	AlN, Al_2O_3	Monolayer graphene	Grown, wet transfer	MBE, MOCVD	Nucleation density is generally higher for AlN than GaN	35,36,42
ZnO	SiC	Monolayer graphene	Grown	Radio-frequency sputtering	Graphene buffer layer is used	33
STO	STO	Two-layer graphene	Dry transfer	PLD	High-temperature growth results in the worst yield out of all complex-oxide materials	3
CFO	MAO	One or two-layer graphene	Dry transfer	PLD	Owing to the low-temperature growth condition, monolayer graphene also works	3
YIG	GGG	Two-layer graphene	Dry transfer	PLD	Post annealing helps improve crystallinity	3
BTO	STO	Monolayer graphene	Dry transfer, wet transfer	MBE	Using ozone as an oxygen source will instantly etch graphene	3
$CsPbBr_3$	NaCl	Monolayer graphene	Wet transfer	CVD	Modified wet transfer process is used	48
VO_2	Al_2O_3	Monolayer graphene	Wet transfer	PLD	Post annealing of the epitaxial film is needed	131
$LiNbO_3$	Al_2O_3	Monolayer graphene	Wet transfer	PLD	Post annealing of the epitaxial film is needed	132
Copper	Al_2O_3	Monolayer graphene	Wet transfer	Thermal evaporation	Before the growth, the vacuum chamber was coated with copper film to block any contaminations	133
GdPtSb	Al_2O_3	Monolayer graphene	Wet transfer	MBE	Successfully exfoliated without the need for a metal stressor layer	66
HfS_2	Al_2O_3	One or two-layer h-BN	Wet transfer	CVD	Modified wet transfer process; photodetectors are demonstrated; h-BN is used as an interlayer	134
ZnO (nanorod)	Polycrystal ZnO	Monolayer graphene	Wet transfer	Hydrothermal method	Lattice transparency of graphene is reduced by increased graphene thickness	135
ZnO (micro-rod)	ZnO on r-Al_2O_3 and c-GaN	One to three-layer graphene	Wet transfer	Hydrothermal method	High-temperature annealing is required to heteroepitaxially crystallize the spin-coated ZnO layer on r-Al_2O_3 and c-GaN substrates	59
ZnO (nanorod)	ZnO nanorod	Monolayer MoS_2	Wet transfer	Hydrothermal method	Remote epitaxy is conducted on nanorods; MoS_2 is used as an interlayer	136
ZnO (rod, disc, needle)	GaN	One to three-layer graphene	Wet transfer	Hydrothermal method	Morphology is controlled by chemicals and additives, and position can be controlled by mask patterns	60,61,64,65
GaN (rod, polyhedron)	Al_2O_3	One or two-layer graphene	Wet transfer	MOCVD	High III/V molar flow ratio is needed to form rod-shaped structures	16,17,41
GaN (polyhedron)	AlN	Monolayer graphene	Wet transfer	MOCVD	Nuclei emerge from triangular to hexagonal shape	17
GaN (tetrahedron)	SiC	Monolayer graphene	Grown	MOCVD	Pre-annealing treatment in H_2/NH_3 mixture environment is required to grow remote epitaxial structures before the nucleation step	40

Al_2O_3, sapphire; BTO, barium titanate; CFO, cobalt ferrite; CVD, chemical vapour deposition; GaN, gallium nitride; GGG, gadolinium gallium garnet; h-BN, hexagonal boron nitride; MAO, magnesium aluminate; MBE, molecular beam epitaxy; MOCVD, metal–organic chemical vapour deposition; NH_3, ammonia; PLD, pulsed laser deposition; STO, strontium titanate.

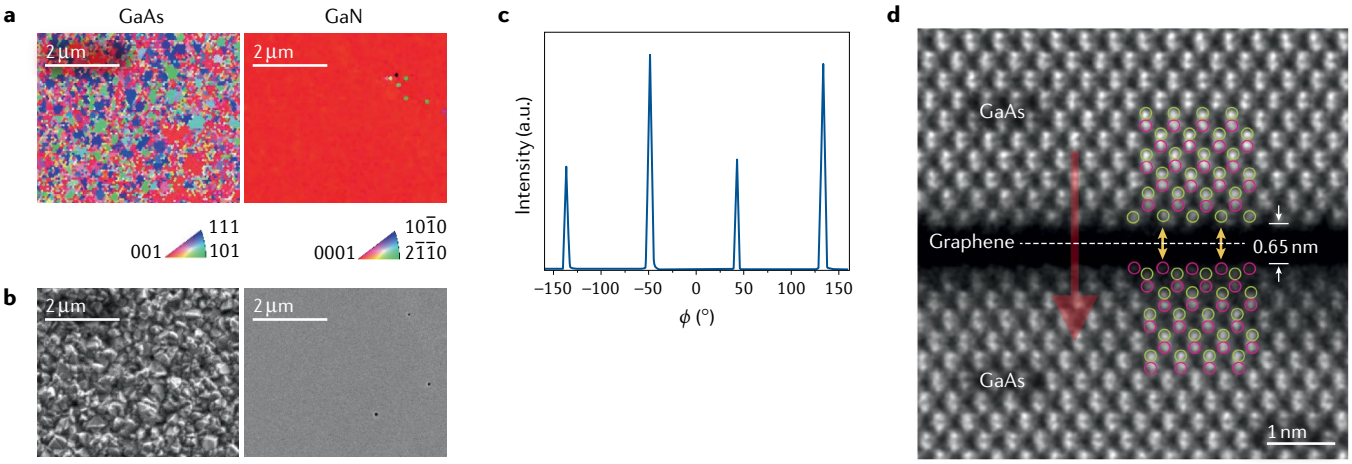

Fig. 4 | **Characterization of remote epitaxial thin films. a** | Electron backscatter diffraction (EBSD) map of bilayer graphene-coated GaAs and gallium nitride (GaN). **b** | Scanning electron microscopy (SEM) images of corresponding films. **c** | High-resolution X-ray diffraction (XRD) φ-scan of exfoliated GaAs film showing fourfold symmetry. **d** | Cross-sectional scanning transmission electron microscopy (STEM) image of GaAs/graphene/GaAs. φ, rotation of the sample. Parts **a** and **b** reprinted from REF.[15], Springer Nature Limited. Part **c** adapted from REF.[12], Springer Nature Limited. Part **d** reprinted with permission from REF.[31], AIP.

spectroscopy in STEM mode, chemical information about the film can be derived. Diffraction patterns acquired in the TEM mode can identify different crystallographic domains in cross section. This can also be visualized as a false-colour map to show the distribution of differently oriented domains[94].

As a representative example, the characterization of GaAs (III–V) and GaN (III–N) films grown on bilayer graphene transferred on GaAs and GaN, respectively, is shown in FIG. 4. The EBSD map in FIG. 4a reveals crystallographic orientations in the GaAs and GaN film. The maps show that, for GaAs, remote epitaxy only works on monolayer graphene, whereas GaN remote epitaxy can be performed with bilayer graphene[15]. SEM images of these films are shown in FIG. 4b. Rough and random facets are observed for the polycrystalline GaAs layer, compared with the smooth surface of single-crystalline GaN. The XRD φ-scan of remote epitaxial GaAs in FIG. 4c shows fourfold symmetry of cubic GaAs grown on monolayer graphene-coated GaAs, confirming that there are no in-plane rotations in these remote epitaxial films. FIGURE 4d shows a cross-sectional HAADF STEM image of GaAs/graphene/GaAs, showing a remote atomic alignment of GaAs through monolayer graphene. Characterization of oxide epitaxial layers is undertaken similarly to III–V or III–N epitaxial layers (shown in Supplementary Fig. 3a–c).

In addition to the remote homoepitaxy of GaAs/graphene/GaAs and GaN/graphene/GaAs, various characterization techniques can reveal remote heteroepitaxy, where the remote epitaxial film exhibits different lattice constants from the substrate. Generally, graphene layers partially screen the substrate potential, weakening the interaction between the substrate and the epitaxial material. This is also the case for halide perovskites grown on NaCl, where the electrostatic potential of the polar NaCl substrate is primarily screened by graphene[48]. When halide perovskite film is grown on a single NaCl substrate with half the region covered by graphene and the other half left empty, the screened substrate electrostatic potential suppresses nucleation of the halide perovskite and promotes growth (shown schematically in FIG. 5a). The topography and atomic structures of the remote epitaxial $CsPbBr_3$ film can be characterized by cross-sectional SEM, cross-sectional HAADF STEM and top-view HAADF STEM (as shown in FIG. 5b,c,d, respectively). Reciprocal space mapping also reveals their epitaxial relations and the film strain, as shown in FIG. 5e for both {224} planes of as-grown $CsPbBr_3$ and NaCl substrate. The weak interaction in remote heteroepitaxy reduces dislocations compared with direct heteroepitaxy without graphene. A similar observation was reported in III–V remote heteroepitaxy[95], suggesting that graphene provides an additional path for strain relaxation.

Remote epitaxially grown microstructures and nanostructures can be characterized using similar methods. The SEM images in FIG. 6a,b show two different microstructures grown by hydrothermal remote epitaxy and MOCVD. Depending on the substrate crystal orientation, unidirectionally aligned horizontal and vertical micro-rods are observed. Meanwhile, MOCVD-grown GaN micro-rods on c-Al_2O_3 are seen to have a 30°-rotated in-plane relationship between the rods and the substrate to minimize the strain by large lattice mismatch, where such rotation also occurs in direct heteroepitaxy of GaN on Al_2O_3 (REF.[16]) (FIG. 6c).

Characterization after 2DLT

After exfoliation, remote epitaxial films or structures and their host substrates can be observed. They should first be examined under an optical microscope to confirm the exfoliated area. When using a nickel stressor layer, the film normally exhibits a different colour from that of nickel. This colour change makes it possible to determine the area, often with the naked eye. Compared with other methods — such as lone use of PMMA or combination with PDMS — where the film is typically transparent or has a slight hue, a nickel stressor makes

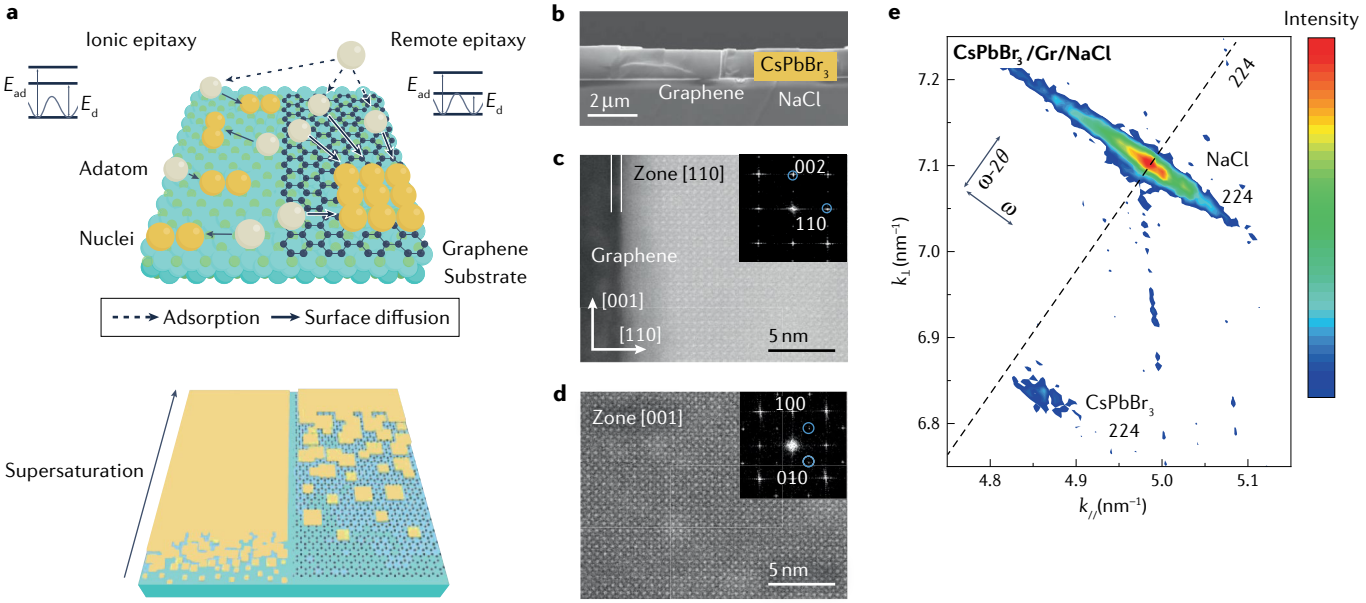

Fig. 5 | **Growth mechanism of ionic and remote epitaxy, and halide perovskite thin film characterization. a** | Atomistic nucleation (top) and supersaturation-dependent morphology (bottom) for both ionic (left) and remote (right) epitaxy. In remote epitaxy, largely suppressed epilayer–substrate interaction reduces the nucleation rate. **b** | Cross-sectional scanning electron microscopy (SEM) image of a remote epitaxial $CsPbBr_3$ thin film on graphene/NaCl. **c** | Cross-sectional scanning transmission electron microscopy (STEM) image of remotely epitaxial $CsPbBr_3$ with zone axis of [1–10]. Smooth interface between $CsPbBr_3$ (bright part) and graphene/NaCl (dark part) shown. **d** | Top-view STEM image of remotely epitaxial $CsPbBr_3$ with zone axis of [001]. Both fast Fourier-transform (FFT) images shown as insets in panels **c** and **d** confirm orthorhombic phase of $CsPbBr_3$. **e** | Reciprocal space mapping of remote epitaxial $CsPbBr_3$ film. Diffraction peaks of 224 for both $CsPbBr_3$ and NaCl shown, indicating an epitaxial relationship of out-of-plane $CsPbBr_3$(001)//NaCl(001) and in-plane $CsPbBr_3$[100]//NaCl[100]. 2θ, diffracted angle; ω, beam incident angle; E_{ad}, adsorption energy; E_d, diffusion energy; $k_{||}$ and $k_\perp$, reciprocal lattice vectors parallel and perpendicular to the substrate surface, respectively. Adapted from REF.[48], CC BY 4.0 (https://creativecommons.org/licenses/by/4.0/).

it easier to determine the region of exfoliated films. As the film colour has a different appearance depending on the material and thickness, regions where the film is partially or fully exfoliated can be identified (see Supplementary Fig. 3a). The peeling efficiency can then be calculated as a fraction of the fully exfoliated area from the initial growth area. If the surface roughness of the epitaxial layer before exfoliation is too high, EBSD mapping can often fail to identify crystallographic orientations. Thus, EBSD is also done at the exfoliated surface, which was once the interfacial layer, to confirm the single-crystallinity of the epitaxial layer (as shown in Supplementary Fig. 3b).

Owing to several factors, such as deposition of the nickel stressor layer, the subsequent adhesion–release processes from the TRT and slight bending of the film during handling, the epilayer can experience strain that forms defects and cracks or generates new domains. The cross-sectional TEM images in Supplementary Fig. 3c, which are measured before and after the nickel stressor deposition, show new crack and defect formation in the epitaxial layer.

Once a thin film is exfoliated, the film gains flexibility depending on the material's Young's modulus. The bending radius can be roughly estimated by observing the bent film's focus change at different regions along a line with an optical profiler using Stoney's equation[96]. The film will crack if the strain caused by the bending radius exceeds the critical crack strain of the material. The characterization of exfoliated microstructures and nanostructures can be conducted similarly. Supplementary Figure 3d shows representative photographs of exfoliated remote epitaxial films and microstructures.

Applications

This section introduces the device applications and functionalities demonstrated by remote epitaxy. As remote epitaxy is still in its early stage of development, efforts and strategies to make the technology more practical and to scale up to system levels are discussed.

Remote epitaxial III–V

Remote epitaxy of III–V and 2DLT enable exfoliation of III–V thin films and hetero-integration with foreign platforms. In general, the growth of III–V on graphene is initiated by a formation of islands, which overgrow and merge to form a planarized thin film. Therefore, growth of III–V device layers on graphene is typically conducted after forming a planarized buffer layer. The first demonstration of remote epitaxial III–V devices was realized on graphene-coated GaAs wafers, by growing red InGaP LEDs with GaAs buffer layers[12]. FIGURE 7a shows the schematic of an LED device directly grown on graphene, with the electrical operation of the LEDs shown in FIG. 7b. The red LEDs were exfoliated from the substrate by 2DLT and then transferred and operated on silicon. The LEDs did not show a significant change in their *I*–*V* and lighting performance before and after exfoliation and transfer (FIG. 7c,d), showing the feasibility of remote epitaxy for hetero-integrated devices.

Remote epitaxy of III–V has so far been demonstrated on GaAs, InP and GaP substrates. As a result, there will not be limitations for applying it to other III–V materials. The proof-of-concept demonstration of remote epitaxy for GaAs/InGaP-based red LEDs indicates that virtually any III–V thin film-based devices can be made free-standing and integrated on foreign platforms. Stand-alone III–V devices — including flexible or curved optoelectronic and photonic devices — can be made by remote epitaxy of III–V and 2DLT. For example, lightweight and high-performance solar cells can be fabricated by remote epitaxy of GaAs and 2DLT, where the metal stressor for 2DLT can work as a back reflector. Free-standing infrared photodetectors and emitters can also be prepared. When integrated with other systems and platforms, there are immense possibilities to boost device performance and enable new functionalities. By combining remote epitaxially made detectors, emitters and solar cells with computing chips, communication chips, light sources and sensors — all of which can be made curved or flexible — technology can be enhanced to produce next-generation displays, augmented/virtual reality, human–machine interfaces and edge computing.

Remote epitaxial III–N

III–N compound semiconductors have been used in various applications, including high-power or radio-frequency transistors, LEDs and laser diodes[37]. Although most applications of III–N are currently implemented on rigid substrates such as silicon, Al_2O_3 or SiC, III–N materials in the form of free-standing films could potentially provide economic benefits or enhanced performance[1]. SiC or high-quality GaN substrates are required to make devices of critical performance, but the material cost often limits the usage compared with Al_2O_3 and silicon. The release of III–N thin films from the substrate immediately allows the reuse of high-value substrates[12,33]. On the other hand, the weak interfacial interactions between the remote epitaxial III–N and 2D material-coated surfaces have been shown to provide improved material quality in the III–N layers. The eradication of dislocations in isolated grains and reduction of dislocations in converged thin films have been observed in III–N remote epitaxy[33,40]. This is an exciting prospect for obtaining high-quality epitaxial devices. In conventional III–N epitaxy, dislocations were inevitable to relax the lattice strain due to the covalently bonded interface[97]. The improvement is thought to result from simultaneously allowing well-aligned crystalline orientation and full relaxation of strain due to the weak coupling at the III–N remote epitaxial interface[95]. Lastly, the decoupling of the remote epitaxial III–N from the rigid substrates also enables the integration of III–N devices with other functional surfaces[71]. So far, remote epitaxy has been used to make efficient deep-ultraviolet LEDs[35,36,42]. High-quality AlN thin films and multi-quantum well structures were epitaxially grown on graphene-coated substrates, showing the improved structural quality of the epitaxial materials and enhanced quantum efficiency of the deep-ultraviolet LEDs. Although the demonstrated applications of III–N remote epitaxy are limited at this stage, the foreseeable implementations of the technology would be in lighting, display, amplifiers and power transistors in the near future.

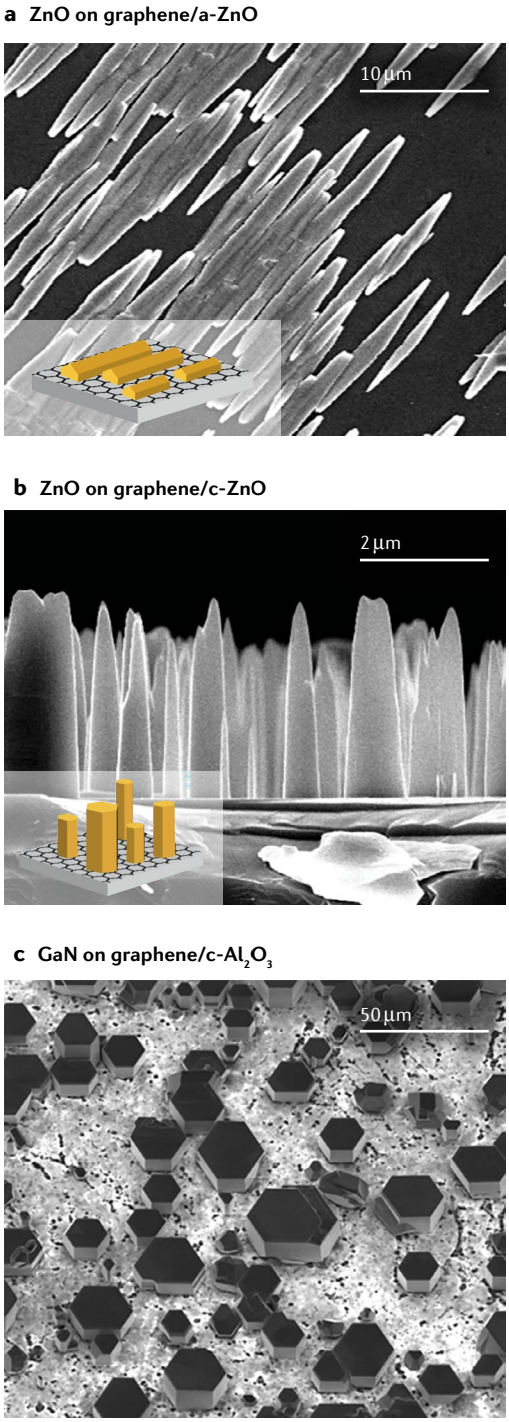

Fig. 6 | **Characterization of microstructures. a** | Scanning electron microscopy (SEM) images of horizontal ZnO micro-rods on graphene/a-ZnO. **b** | Vertical ZnO micro-rods on graphene/c-ZnO. **c** | Gallium nitride (GaN) micro-rods on graphene/c-Al_2O_3. ZnO grown by hydrothermal method, and GaN by metal–organic chemical vapour deposition (MOCVD). Parts **a** and **b** adapted with permission from REF.[59], RSC. Part **c** reprinted with permission from REF.[41], Elsevier.

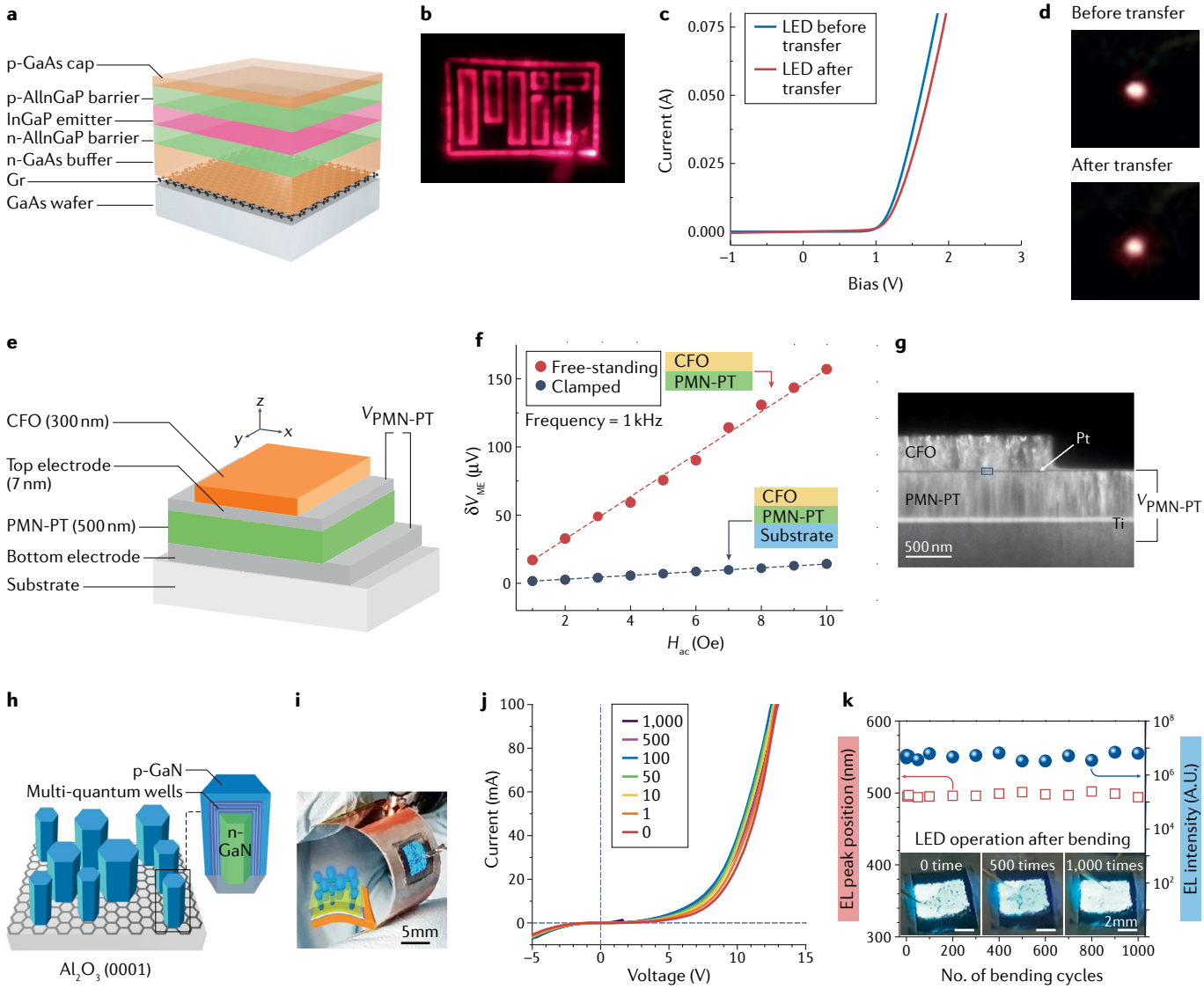

Fig. 7 | **Applications of remote epitaxy. a–d** | InGaP-based red light-emitting diodes (LEDs) fabricated by remote epitaxy: LEDs grown on graphene/GaAs (panel **a**); light emitted from LEDs (panel **b**); *I–V* curves of LEDs grown on graphene–GaAs substrate and directly on GaAs substrate (panel **c**); and light emission of LEDs before and after transfer (panel **d**). **e–g** | Hetero-integrated cobalt ferrite (CFO) and lead magnesium niobate–lead titanate (PMN-PT) membranes: CFO/PMN-PT magnetoelectric device (panel **e**); voltage induced across PMN-PT (δV_{ME}) as a function of alternating-current magnetic field strength at 1 kHz frequency (insets showing free-standing and clamped devices) (panel **f**); and cross-sectional transmission electron microscopy (TEM) image of the CFO/PMN-PT membrane heterostructure (panel **g**). **h–k** | Blue LEDs via remote epitaxy of III–N micro-rods: remote epitaxially grown heterostructured micro-rods (panel **h**); electroluminescence (EL) from bent micro-rod LED (panel **i**); characteristic *I–V* curves measured after repeating bending cycles (1–1,000 times) between radius curvatures ∞ and 10 mm (panel **j**); and EL peak position (red empty squares) and intensity (blue solid circles) measured as a function of bending cycle (panel **k**). LED was flattened and operated at 100 mA after bending cycles. Insets are photographs of EL emission after bending cycles of 0, 500 and 1,000. Al_2O_3, sapphire; GaN, gallium nitride. Parts **b–d** adapted from REF.[12], Springer Nature Limited. Parts **e–g** adapted from REF.[3], Springer Nature Limited. Parts **h–k** adapted with permission from REF.[16], AAAS.

Remote epitaxial complex oxides

Complex oxides embody a wide variety of physical properties such as ferroelectricity, piezoelectricity, pyroelectricity, ferromagnetism, ferrimagnetism, magnetostriction, superconductivity and more. This provides many exciting applications to be demonstrated using flexible, single-crystalline complex-oxide thin films that are detached from the substrate. One application is to stack materials with different physical properties and artificially create a multi-physical heterostructure, a designer heterostructure. For example, a piezoelectric lead magnesium niobate–lead titanate (PMN-PT) can be stacked with magnetostrictive cobalt ferrite ($CoFe_2O_4$, abbreviated CFO) to create a multiferroic heterostructure while maintaining the high piezoelectricity and magnetostrictive coefficient of each material (illustrated in FIG. 7e). Moreover, owing to the extreme thinness of these films, the substrate clamping effect is no longer present, further improving the piezoresponse and magnetostriction. This was demonstrated and showed extremely high strain-mediated magnetoelectric coupling coefficients compared with other works with similar heterostructures[3], as evidenced in FIG. 7f,g.

Pockels coefficient
A coefficient that quantifies the phenomena in which the refractive index of a medium changes proportional to the strength of the applied electric field.

A similar concept is used to prepare free-standing PMN-PT thin films as a versatile platform to impart voltage-controlled stress onto other thin films. Another application of free-standing, complex-oxide thin films is integration with conventional complementary metal-oxide semiconductor (CMOS) platforms or III–V electronic and photonic devices. Some complex-oxide thin films exhibit robust ferroelectricity with ultra-high dielectric constants, making them an ideal gate oxide material for ferroelectric field-effect transistors[98] or negative capacitance field-effect transistors[99]. Owing to the single-crystalline nature, these materials have a high thermal budget and can be incorporated into the fabrication process flow of any conventional CMOS device. Additionally, materials such as barium titanate ($BaTiO_3$, abbreviated as BTO) have an extremely high Pockels coefficient, which enables them to be an excellent platform for high-bandwidth waveguides. BTO can be integrated into SiN waveguides to act as a transducer for quantum information systems[100], which is impossible without epitaxial lift-off and transfer of BTO onto SiN layers.

Remote epitaxial halide perovskites

Over the past two decades, halide perovskites have attracted growing attention owing to their outstanding optoelectronic properties. Demonstrated high-performance devices based on halide perovskites include photovoltaics[50], LEDs[51], lasers[52], photodetectors[101] and transistors[102]. For most practical applications of semiconducting devices, epitaxial thin films are preferred. Epitaxial films of halide perovskites show supercarrier dynamics[56], high optoelectronic performance[53–55] and better phase stability[57,103] over the polycrystalline counterpart. Remote epitaxy allows the development of an epitaxial halide film with low dislocation density and better optoelectronic quality. Recently, it has been experimentally demonstrated that, compared with the epitaxial $CsPbBr_3$ film directly grown on NaCl, remote epitaxially grown $CsPbBr_3$ shows improved photoresponse when used in a two-terminal photodetector[48]. This has been attributed to the low optically active defect density — the threading dislocation density — in the remote epitaxial film. With increased understanding and knowledge of the atomistic mechanism and processing of remote epitaxy in halide perovskites, more applications are expected to emerge.

In general, thin films (a few hundred nanometres or thinner) have a much higher elastic strain limit than their bulk forms — typically three orders of magnitudes for ceramics — due to the size effect of crystalline materials associated with the elastic strain limit[104]. Epitaxial halide perovskites films with high crystallinity and low-density defects can be integrated on any electronically active, optically active or mechanically flexible substrate using remote epitaxy and subsequent transfer. This enables a much larger design space for developing future perovskite halide-based functional devices, as suggested in Supplementary Fig. 4.

Remote epitaxial microstructures/nanostructures

Spatially isolated microstructures or nanostructures fabricated by remote epitaxy provide an ideal geometry for transferable, deformable and bespoke devices. Furthermore, the host wafers can be reused after 2DLT without an elaborate surface refurbishing process, such as chemical or mechanical polishing. One of the desired device applications is to create a large, flexible lighting panel with numerous blue LED-architectured micro-rod arrays. This can be achieved by remote epitaxy of III–N micro-rods[16,41]. For LED operation, micro-rods of n-type core and outermost p-type shells are made and embedded with InGaN/GaN multi-quantum wells (FIG. 7h). The grown micro-rods are encapsulated by PI. The top and bottom electrodes are formed at both sides of PI, contacting the p and n-segments of the micro-rods for electrical injection. The PI-encapsulated micro-rod LEDs can be transferred onto a conductive, deformable metal plate through the transfer process using TRT. The blue LED panel attached to copper foil or tape is tolerant against various deformations, such as bending, crumpling and folding (FIG. 7i). The bending deformations can be repeated more than 1,000 times at bending radii between ∞ and 10 mm, without any apparent degradation in electrical properties, electroluminescence (EL) intensities and emission wavelengths[16] (FIG. 7j,k). Matrix arrays of micro-rod LED panels are also demonstrated, where the LED arrays show uniform emission properties without degradation by deformations[41].

Another advantage of remote epitaxy is that the donor wafers can be reused. After 2DLT, the wafers can be recycled for another remote epitaxy by simply removing the graphene with oxygen plasma treatment, followed by standard wet cleaning of the wafer. Then, the overall procedure of remote epitaxy — graphene transfer and MOCVD of micro-rod LED arrays — can be carried out on the cleansed wafer. Notably, LEDs with comparable quality are obtained from reused wafers[16]. Such wafer reusability can significantly reduce manufacturing costs and could be important for carbon-neutral production of electronics and optoelectronics.

Building hetero-integrated systems

Remote epitaxy enables manufacturing of high-quality thin films and structures that can be detached from the host wafers and made in free-standing forms. This provides a path for hetero-integration of electronic and optoelectronic devices of high performances, such as LEDs, photodiodes and high electron-mobility transistors, which could not be grown on the same substrate owing to the lattice-matching requirement. Such hetero-integration schemes can be further expanded to a system-level hetero-integration that incorporates multiple, stackable thin films as individual functional building blocks, enabling artificial intelligence (AI) chips, wireless communications, sensors, micro-batteries and solar cells. Leveraged by the high degree of freedom for electronic functions, geometries and places, the implementation of artificial heterostructure systems can be harnessed in various fields. Example applications include optoelectronic systems, neuromorphic computing systems and skin electronics.

Multifunctional optoelectronic thin films can be individually transferred and stacked to any substrate. This enables the heterostructure system to incorporate optoelectronic functions, such as multispectral colour

display, optical communication and image sensing. One potential example is a multispectral focal plane array (MSFPA) that allows for the visual detection of multiple wavelengths such as visible, infrared, short-wave infrared and ultraviolet[105,106]. Pieces of information from each spectrum can be extracted and combined in MSFPAs to create meaningful information. For instance, infrared lights can be generated by black-body radiation of the target objects. Combining the independent visible and infrared information enables enhanced night vision by the machine learning-based spectral fusion algorithms[107,108]. For fabrication of MSFPAs, a large-scale focal plane array requires silicon-based CMOS read-out circuitry, whereas the optoelectronic active pixels generally incorporate III–V compound semiconductors. Multiple layers of III–V detectors with different spectral sensitivities can be stacked and hetero-integrated on CMOS circuitry by remote epitaxy and 2DLT. Consequently, this approach could replace the conventional macroscale metal–wire interconnections, which induce undesired power dissipation and signal delay through parasitic inductance and capacitance. This could provide a path for smaller feature sizes, improved parasitic effect and lower system costs.

As another example, neuromorphic computing is an emerging bio-inspired computing technique proposed as an alternative to silicon electronics with the issue of further scalability[109–111]. The increasing data size from the massive applicability of AI, computer vision and big data requires a more efficient computing platform than the conventional central processing units and graphic processing units. Instead of employing 0 and 1 binary variables, neuromorphic computing incorporates a multistate analogue computing capability based on intelligent matters such as memristors, ferroelectric devices, magnetic devices and ionic electrolyte transistors[112]. These intelligent devices enable in-memory computing attributed to storing information in the physical material medium that simultaneously features arithmetic operations for AI computing. Such devices are generally incorporated as a crossbar array to process large-scale data, where additional CMOS read-out circuitry is required, similar to the MSFPA system. Remote epitaxy technology is ideal for hetero-integration of intelligent matters with silicon electronics, which opens new opportunities to implement compact neuromorphic chips while minimizing complex fabrication processes.

Lastly, bio-inspired systems require a flexible substrate that can be easily attached and transplanted to curvy and deformable human bodies[105,113,114]. Therefore, intact flexible and stretchable systems can maximize the acquisition of imperceptible signals and could provide promising surgical treatments and non-invasive diagnosis in conjunction with AI algorithms[115]. Flexible sensing platforms can be realized through various sensing materials, including III–V compound semiconductors and piezoelectric and piezoresistive materials, such as lead zirconate titanate (PZT), polyvinylidene fluoride–trifluoroethylene (PVDF-TrFE) and poly (3,4-ethylenedioxythiophene) polystyrene sulfonate (PEDOT:PSS)[116–119]. With remote epitaxy as a base technique, it is possible to incorporate paper-cutting structures, also known as kirigami or origami arts, allowing 3D transformable geometries that possess shape tunability, high pixel fill factor and bendability. This provides tunable device performance[114,120]. Furthermore, multiple remote epitaxy processes enable the transfer of stacked sensing materials onto a conformal substrate, which could apply to various functional devices, such as beam steering, artificial eyes, 2D/3D mixed-dimensional devices and non-line-of-sight detection[121,122].

In summary, remote epitaxy processes can offer a high degree of freedom for hetero-integration. The potential branches can also be co-designed, providing synergistic effects to realize further advanced systems.

Reproducibility and data deposition

The reproducibility of remote epitaxy and 2DLT is critically important for the reliable production of high-quality, single-crystal thin films and structures. Reproducibility is primarily affected by several factors related to preparation processes for graphene-coated templates, remote epitaxy processes and 2DLT processes[1,4,30,71]. The most important step is the preparation of graphene-coated templates, which are generally conducted by 2D material formation on foreign substrates and then transfer onto the target substrate. When graphene is grown, either on foreign substrates or directly on the target substrate, if there is an irregular graphene thickness greater than the critical distance for remote interaction, then remote interaction through the graphene layer is not possible in that region[15,30]. Thick graphene leads to low density of nucleation, which will be partially polycrystalline, making it challenging to grow fully planarized single-crystalline thin films. Therefore, the graphene layer thickness and uniformity must be carefully controlled and characterized before remote epitaxy. Next, defects and pinholes in graphene, often formed during the transfer processes, trigger covalent bonding between epilayers and substrates[3,12]. In other words, direct epitaxy occurs from the defective area, and the region cannot be exfoliated smoothly because of the strong covalent bonds at the interface[12], as shown in the SEM images in FIG. 8a,b. Furthermore, several disorders can be involved during the transfer process, such as nanometre- to micrometre-scale pinholes, wrinkles, ripples and non-pristine interfaces, severely disturbing remote interaction. Therefore, minimizing the contamination and damage during the graphene growth and transfer is key to reproducible and reliable remote epitaxy[31,43]. In this regard, directly growing graphene on the substrates of interest would be ideal for reliable remote epitaxy and substrate recycling (see Supplementary Fig. 3e). Direct growth does not involve the transfer processes, meaning graphene uniformity can be directly controlled by tailoring chemical reactions during growth[33,34]. However, the stability of substrates at the graphene growth temperature needs to be considered[45,123].

During remote epitaxy, the epitaxy environment needs to be monitored for reproducible film quality. To do this, sensors in the epitaxy tools — such as thermocouples, pyrometers, RHEEDs, reflectometers, residual gas analysers or others — should be used to ensure that

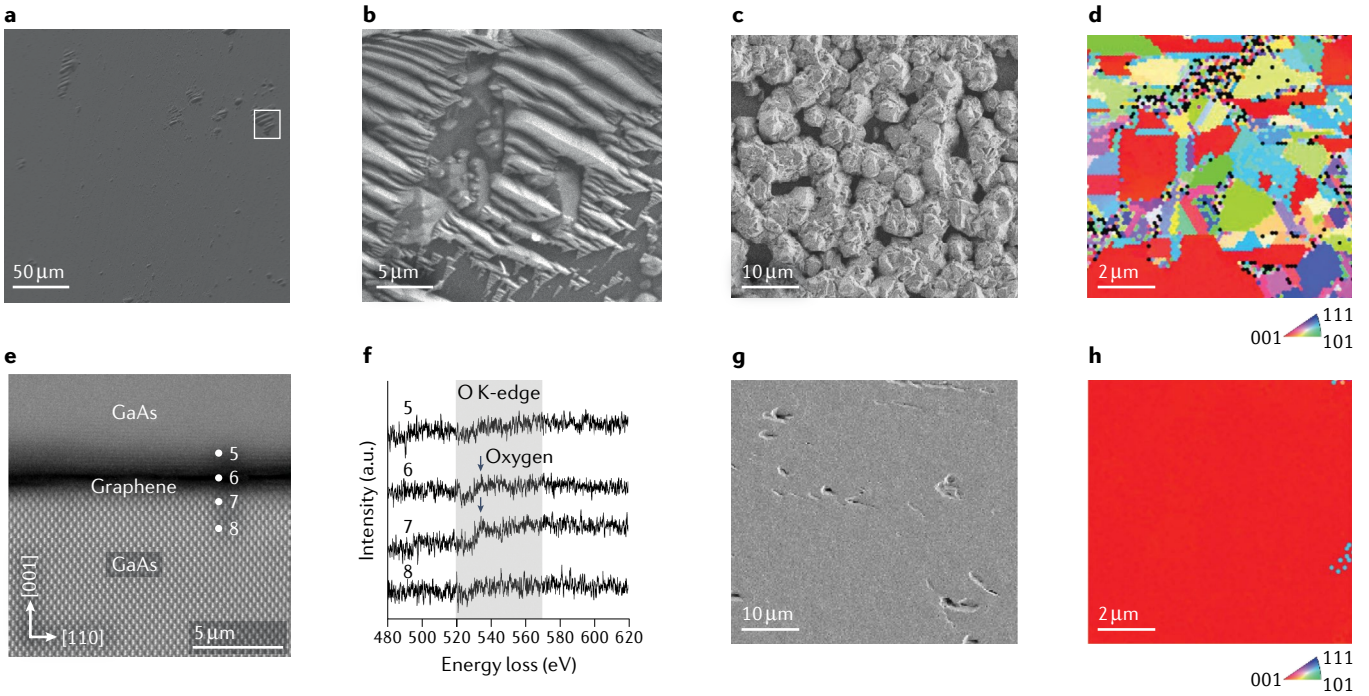

Fig. 8 | **Challenges in remote epitaxy. a** | Scanning electron microscopy (SEM) image of GaAs substrate after remote epitaxy and layer transfer. Holes in graphene induce spalling of substrates. **b** | SEM image of substrate spalling in dashed box in panel **a**. **c**–**e** | GaAs grown on wet-transferred graphene imaged by SEM (panel **c**); electron backscatter diffraction (EBSD) mapping (panel **d**); and cross-sectional scanning transmission electron microscopy (STEM) (panel **e**). **f** | Electron energy loss spectroscopy spectra of oxygen K-edge showing presence of interfacial oxide. Each spectrum extracted at points marked in panel **e**. **g**,**h** | GaAs grown on dry-transferred graphene by metal–organic chemical vapour deposition (MOCVD) using H_2 carrier imaged by SEM (panel **g**) and EBSD mapping (panel **h**). Parts **a** and **b** adapted from REF.[12], Springer Nature Limited. Parts **c**, **d**, **g** and **h** adapted with permission from REF.[30], ACS. Parts **e** and **f** reprinted with permission from REF.[31], AIP.

growth conditions do not drift or fluctuate. Remote epitaxy conditions often involve harsh environments, such as high temperatures and reactive gases. As a result, preserving the graphene layer in these environments is an important requisite for the reproducible production of remote epitaxial films.

The reproducibility of the 2DLT process strongly depends on the stressor condition, the adhesion energy between the stressor and epilayers, and the vdW interface[14,16,70,124]. The stress condition governs the generation and propagation of cracks, and thus the stress level and thickness of the nickel stressor layer need to be well controlled. Typically, nickel is deposited by direct current sputtering. The chamber pressure and sample temperature can be manipulated to tune the stress level of nickel. It is also important to preserve sufficient adhesion energy between epilayers and stressor layers[14,15,48]. Insufficient adhesion energy produces self-delamination of the stressor layer from the epilayer, not at the graphene interface[1,95]. Therefore, depositing a thin adhesion layer, such as titanium or chromium, before nickel sputtering can ensure strong adhesion at the interface. In summary, for a reproducible process, it is necessary to start with a uniformly covered, pristine graphene layer, which is preserved during remote epitaxy, with careful monitoring of the epitaxy environment and stressor deposition conditions.

Currently, research on remote epitaxy is in the early stages. High-yield and reproducible manufacturing processes are not yet well established, especially for materials with weak ionicity[15]. For reliable remote epitaxy and free-standing thin film production, it is crucial to conduct each experimental process with rigorous characterizations at each step to ensure that the results can be directly correlated to the experimental conditions.

Limitations and optimizations

Challenges in remote epitaxy

The biggest challenge in ensuring successful remote epitaxy is obtaining consistent, large-area, high-quality graphene. It is well known that growing graphene with high consistency over a large area is difficult because the Gibbs free energy remains relatively consistent, leading to the simultaneous formation of single, double and, possibly, multilayered materials with the same free energy on the substrate[22,125]. If there are areas with thick graphene, those areas will result in the formation of polycrystalline films during remote epitaxy, significantly reducing the crystal quality. These areas of non-uniform thickness can be incredibly hard to detect as they may be several nanometres in size. Finding a method to grow monolayer, pristine, large-area graphene is of the utmost importance and urgency. The most optimal growth would be a self-limited growth mode where, thermodynamically, only one or two monolayers of graphene can be grown, such as on SiC substrates.

The next challenge is the transfer step. It is still very challenging to transfer large-area graphene onto

foreign substrates. Transferred graphene often exhibits organic residues with many macroscopic defects such as tears and wrinkles, which reduce the exfoliation area yield during the 2DLT process. The wet transfer process, which is the most widely used technique for transferring graphene, induces oxidation of substrates due to trapped water underneath graphene because it is raised from water. This can result in remote epitaxy failing, as shown in the case of GaAs remote epitaxy on wet-transferred graphene in FIG. 8c,d. Cross-sectional TEM and electron energy loss spectroscopy measurements revealed interfacial oxides, preventing remote epitaxy[30] (FIG. 8e,f). The dry transfer method alleviates some of these issues, but some variations and mistakes inevitably occur because humans perform it. Obtaining pristine large-area graphene and transferring it onto a foreign substrate go hand in hand in difficulty. A robust transfer process for each semiconductor or complex-oxide material is still being optimized to reduce remnant residues and macroscopic tears, wrinkles and folds on the graphene surface.

Another issue may arise when the substrate is highly reactive to polar solvents, such as water. Lithium-based materials may be sensitive to moisture, which prevents the transfer of graphene using any polar solvents. A solution to this issue is to transfer graphene purely in non-polar solvents such as IPA. This method requires several steps. The first step is to transfer SiC-graphene onto a SiO_2/silicon platform using the dry transfer technique. Next is to use PMMA as a handling layer and etch the SiO_2 in buffered oxide etchant (BOE), rinsing the PMMA/graphene film in deionized water and, then, transferring the film to IPA. The final step is to dip the reactive substrate into IPA and transfer the PMMA/graphene onto the reactive substrate. The IPA can then be drained, leaving the PMMA/graphene/substrate stack. The PMMA can be dissolved in acetone, leaving behind the graphene/substrate stack.

Finally, remote epitaxy is limited by the growth conditions. If epitaxial growth occurs in an environment where graphene is damaged, remote epitaxy cannot be conducted successfully. For example, the SEM and EBSD images in FIG. 8g,h show that remote epitaxy of GaAs fails when GaAs is grown by MOCVD using a hydrogen carrier because graphene is damaged under such growth conditions[30]. The quality of remote epitaxial thin films is more severely affected by the graphene and environment in materials with lower ionicity because of the weaker electrostatic potential fluctuation on graphene that guides the nucleation. Fortunately, most materials can be epitaxially grown using MBE, which is an excellent tool for remote epitaxy. The growth conditions are sufficiently mild, even at high temperatures, for remote epitaxy of III–V, III–N and complex-oxide materials. For growth using tools such as PLD — which may damage the graphene owing to the plasma at high temperatures — one way to prevent graphene damage is to perform a slightly off-axis deposition. This means the graphene/substrate stack is not directly above the plasma plume but at a slight angle. However, off-axis deposition is limited as epitaxial growth while maintaining a perfect stoichiometry may not be possible in this set-up.

2DLT and device fabrication challenges

2DLT is a universal transfer method for creating heterointegrated electronic and photonic systems. Scaling up 2DLT for industrial applications is limited because heterogeneous integration by remote epitaxy has only been demonstrated on a small scale. Therefore, developing a reliable and systematic 2DLT process at a large scale is imperative.

Fabrication of a high-performance device requires a graphene layer with a low defect density. Defects in graphene, such as cracks and pinholes, cause direct exposure of the substrate to adatoms, resulting in direct bonding of the epitaxial layer to the substrate. The direct bonding without 2D materials results in a destructive spalling exfoliation instead of 2DLT. This unintentionally generates rough morphology and spalling marks on the substrate and transferred layer[12]. As it is challenging to grow large-scale, high-quality graphene and transfer it without damage, directly growing graphene or other 2D layers on substrates for remote epitaxy could be investigated.

Other challenges relate to exfoliation and handling stability. The 2DLT technique requires a nickel stressor layer. However, the additional nickel deposition process can damage the originally transferred material structures. As the nickel deposition is generally performed by sputtering and ion bombardment, the increase in sample temperature during sputtering could cause contamination or film degradation. As a result, unless the film is comparatively thick (micrometre scale), additional protective layers on the film surface could alleviate these challenges by minimizing possible stoichiometric and atomic interactions between the nickel stressor and the film.

Stable exertion of uniform forces during attachment and release ensures reliable film transfer. However, depending on the thickness of the remote epitaxial film, it can crack during exfoliation. Minor differences in the procedure can affect the results of 2DLT and transfer onto foreign substrate. Consequently, an automated exfoliation set-up capable of mimicking the process with precise controllability of parameters in the peeling process is required to guarantee consistent exfoliation results at a given stress condition. A capillary transfer technique was recently proposed that uses a liquid-assisted natural adhesion between soft films and solid substrates, minimizing the variations during handling[126]. Another recent study on 2D to 3D transformation and transfer via anchoring and liquid-level modulation could also aid in achieving high transferability[127]. Furthermore, mechanical simulations for the automation can be used to determine the parameters for the automated system and to realize a stable and repeatable transfer platform, which could overcome these challenges and reliably produce high-performance devices and platforms by remote epitaxy.

Outlook

Remote epitaxy is a new epitaxy concept, involving vdW interlayers. The method has a short history since its first report in 2017. The discovery of remote epitaxy has opened up many exciting opportunities for device

applications and as a tool to study fundamental science. For functional devices and applications, remote epitaxy enabled the growth and separation of single-crystal thin films from the wafer, which was feasible for a limited choice of materials using conventional approaches. The role of the vdW interlayer, typically graphene, is not limited to a releasable interface but also provides a ground for strain relaxation that can improve the quality of the grown material. The features facilitated by remote epitaxy and 2DLT make it a promising approach for flexible, bendable or ultra-thin applications and hetero-integrated systems. Additionally, the 3D–2D–3D material system with crystallographic relationships is an ideal platform to study the underlying physics of mixed-dimensional heterostructures. This includes analysis of physical, electric, magnetic and chemical couplings, alongside atomic interactions.

Although remote epitaxy and 2DLT offer exciting opportunities, experimental demonstration — growth of high-quality single-crystal thin films and structures on substrates coated with 2D materials, followed by exfoliation at the 2D interface — requires stringent experimental conditions owing to the extreme sensitivity of remote interactions at the atomic scale. In this Primer, a comprehensive guide is provided for successful remote epitaxy. First, the methods used to prepare graphene as a vdW interlayer on substrates were introduced. The importance of the thickness, quality and transfer process of graphene was explained in detail, with strategies to prepare graphene on each substrate material. Next, the epitaxy processes were discussed in detail to grow high-quality remote epitaxial films and structures without damaging the graphene layer. Lastly, step by step methods to exfoliate the grown layer at the interface by 2DLT were introduced to use the grown layer for diverse functional and hetero-integrated device applications.

Successful experimental demonstration of remote epitaxy has been achieved for many material systems, including III–V, III–N, II–VI, I–VIII, complex oxides, halide perovskites and metal. In addition, a theoretical understanding of the remote epitaxy mechanism has been enriched by density functional theory and molecular dynamics simulations. These simulations explain why remote epitaxy does or does not work under certain conditions. Although the field is rapidly growing, there remain many challenges to overcome. As a future direction, for more reliable and scalable processes, it is envisioned that the transfer processes of vdW materials need to be eliminated, particularly for device applications and the reuse of substrates. This is because residue and defect formation is inevitable during transfer. In this regard, remote epitaxy on the substrate with directly grown vdW material is an ideal approach, which has been demonstrated on a limited choice of materials: III–N on graphitized SiC and CVD-grown graphene-coated Al_2O_3. For many other substrates, the substrate material cannot sustain the high growth temperature of graphene, typically higher than 900–1,000 °C. Therefore, a low-temperature growth process needs to be developed for those materials. Fortunately, recent reports demonstrate low-temperature growth of atomically thin sp^2-bonded vdW materials[28], which could be adopted as a promising approach.

In summary, remote epitaxy isolates single-crystal thin films and structures from wafers, which was previously impossible or impractical for many materials. Although this technology is still in its early stages, with experimental challenges to overcome, the library of materials that can be made free-standing by remote epitaxy is quickly growing. Many studies are currently focused on material investigation rather than device applications, but it is evident that once remote epitaxy matures it will enable novel functionalities by decoupling the epitaxial layer from the host substrate and establishing a new coupling of dissimilar materials by 2DLT and stacking. This could revolutionize the field of sensor fusion, multifunctional AI, edge computing and bioelectronics, to name a few.

Published online: 01 June 2022

1. Kum, H. et al. Epitaxial growth and layer-transfer techniques for heterogeneous integration of materials for electronic and photonic devices. *Nat. Electron.* **2**, 439–450 (2019).
This review introduces existing techniques for layer transfer of single-crystalline membranes.
2. Yoon, J. et al. GaAs photovoltaics and optoelectronics using releasable multilayer epitaxial assemblies. *Nature* **465**, 329–333 (2010).
3. Kum, H. S. et al. Heterogeneous integration of single-crystalline complex-oxide membranes. *Nature* **578**, 75–81 (2020).
This paper shows remote epitaxy and 2DLT of complex oxides, from which artificial heterostructures are formed by directly stacking free-standing membranes.
4. Geim, A. K. & Grigorieva, I. V. Van der Waals heterostructures. *Nature* **499**, 419–425 (2013).
5. Horowitz, K. A., Remo, T. W., Smith, B. & Ptak, A. J. *A Techno-Economic Analysis and Cost Reduction Roadmap for III–V Solar Cells*. Technical Report NREL/TP-6A20-72103 (National Renewable Energy Laboratory, 2018).
6. Cheng, C. W. et al. Epitaxial lift-off process for gallium arsenide substrate reuse and flexible electronics. *Nat. Commun.* **4**, 1–7 (2013).
7. Lu, D. et al. Synthesis of freestanding single-crystal perovskite films and heterostructures by etching of sacrificial water-soluble layers. *Nat. Mater.* **15**, 1255–1260 (2016).
8. Bakaul, S. R. et al. Single crystal functional oxides on silicon. *Nat. Commun.* **7**, 1–5 (2016).
9. Raj, V. et al. Layer transfer by controlled spalling. *J. Phys. D Appl. Phys.* **46**, 152002 (2013).
10. Bedell, S. W., Lauro, P., Ott, J. A., Fogel, K. & Sadana, D. K. Layer transfer of bulk gallium nitride by controlled spalling. *J. Appl. Phys.* **122**, 025103 (2017).
11. Wong, W. S., Sands, T. & Cheung, N. W. Damage-free separation of GaN thin films from sapphire substrates. *Appl. Phys. Lett.* **72**, 599 (1998).
12. Kim, Y. et al. Remote epitaxy through graphene enables two-dimensional material-based layer transfer. *Nature* **544**, 340–343 (2017).
This paper presents the first demonstration of remote epitaxy, proving that epitaxy can remotely occur through graphene.
13. Novoselov, K. S. et al. Electric field in atomically thin carbon films. *Science* **306**, 666–669 (2004).
14. Shim, J. et al. Controlled crack propagation for atomic precision handling of wafer-scale two-dimensional materials. *Science* **362**, 665–670 (2018).
This paper demonstrates the principles of 2DLT and the role of stressor layers, which are theoretically investigated and experimentally shown.
15. Kong, W. et al. Polarity governs atomic interaction through two-dimensional materials. *Nat. Mater.* **17**, 999–1004 (2018).
This paper investigates the impact of material polarity on the strength of remote interaction, which reveals the limits on the interlayer thickness for remote epitaxy.
16. Jeong, J. et al. Remote heteroepitaxy of GaN microrod heterostructures for deformable light-emitting diodes and wafer recycle. *Sci. Adv.* **6**, eaaz5180 (2020).
This paper reports flexible blue LEDs realized by remote epitaxy of GaN micro-rods.
17. Qu, Y. et al. Long-range orbital hybridization in remote epitaxy: the nucleation mechanism of GaN on different substrates via single-layer graphene. *ACS Appl. Mater. Interfaces* **14**, 2263–2274 (2022).
18. Li, X. et al. Large-area synthesis of high-quality and uniform graphene films on copper foils. *Science* **324**, 1312–1314 (2009).
19. Emtsev, K. V. et al. Towards wafer-size graphene layers by atmospheric pressure graphitization of silicon carbide. *Nat. Mater.* **8**, 203–207 (2009).
20. Nguyen, V. L. et al. Layer-controlled single-crystalline graphene film with stacking order via Cu–Si alloy formation. *Nat. Nanotechnol.* **15**, 861–867 (2020).
21. Wang, M. et al. Single-crystal, large-area, fold-free monolayer graphene. *Nature* **596**, 519–524 (2021).
22. Kong, W. et al. Path towards graphene commercialization from lab to market. *Nat. Nanotechnol.* **14**, 927–938 (2019).
23. Lee, J. H. et al. Wafer-scale growth of single-crystal monolayer graphene on reusable hydrogen-terminated germanium. *Science* **344**, 286–289 (2014).

24. Hwang, J. et al. Van der waals epitaxial growth of graphene on sapphire by chemical vapor deposition without a metal catalyst. *ACS Nano* **7**, 385–395 (2013).
25. Chen, Z. et al. Direct growth of wafer-scale highly oriented graphene on sapphire. *Sci. Adv.* **7**, eabk0115 (2021).
26. Wang, H. et al. Primary nucleation-dominated chemical vapor deposition growth for uniform graphene monolayers on dielectric substrate. *J. Am. Chem. Soc.* **141**, 11004–11008 (2019).
27. Chen, Z., Qi, Y., Chen, X., Zhang, Y. & Liu, Z. Direct CVD growth of graphene on traditional glass: methods and mechanisms. *Adv. Mater.* **31**, 1803639 (2019).
28. Toh, C. T. et al. Synthesis and properties of free-standing monolayer amorphous carbon. *Nature* **577**, 199–203 (2020).
29. Hong, S. et al. Ultralow-dielectric-constant amorphous boron nitride. *Nature* **582**, 511–514 (2020).
30. Kim, H. et al. Impact of 2D–3D heterointerface on remote epitaxial interaction through graphene. *ACS Nano* **15**, 10587–10596 (2021).
This paper unveils the impact of graphene transfer methods and interface properties on remote epitaxy.
31. Kim, H. et al. Role of transferred graphene on atomic interaction of GaAs for remote epitaxy. *J. Appl. Phys.* **130**, 174901 (2021).
32. Phillips, J. C. Ionicity of the chemical bond in crystals. *Rev. Mod. Phys.* **42**, 317 (1970).
33. Qiao, K. et al. Graphene buffer layer on SiC as a release layer for high-quality freestanding semiconductor membranes. *Nano Lett.* **21**, 4013–4020 (2021).
This paper shows the use of transfer-free graphene and graphene buffer on SiC for remote epitaxy and substrate reuse.
34. Kim, J. et al. Principle of direct van der Waals epitaxy of single-crystalline films on epitaxial graphene. *Nat. Commun.* **5**, 4836 (2014).
35. Chen, Z. et al. Improved epitaxy of AlN film for deep-ultraviolet light-emitting diodes enabled by graphene. *Adv. Mater.* **31**, 1807345 (2019).
36. Chang, H. et al. Quasi-2D growth of aluminum nitride film on graphene for boosting deep ultraviolet light-emitting diodes. *Adv. Sci.* **7**, 2001272 (2020).
37. Morkoç, H. *Handbook of Nitride Semiconductors and Devices: Material Properties, Physics and Growth* Vol. 1 (Wiley-VCH, 2009).
38. Tarsa, E. J. et al. Homoepitaxial growth of GaN under Ga-stable and N-stable conditions by plasma-assisted molecular beam epitaxy. *J. Appl. Phys.* **82**, 5472 (1998).
39. Hiramatsu, K. et al. Growth mechanism of GaN grown on sapphire with A1N buffer layer by MOVPE. *J. Cryst. Growth* **115**, 628–633 (1991).
40. Journot, T. et al. Remote epitaxy using graphene enables growth of stress-free GaN. *Nanotechnology* **30**, 505603 (2019).
41. Jeong, J. et al. Transferable, flexible white light-emitting diodes of GaN p–n junction microcrystals fabricated by remote epitaxy. *Nano Energy* **86**, 106075 (2021).
42. Wang, P. et al. Graphene-assisted molecular beam epitaxy of AlN for AlGaN deep-ultraviolet light-emitting diodes. *Appl. Phys. Lett.* **116**, 171905 (2020).
43. Ren, F. et al. Van der Waals epitaxy of nearly single-crystalline nitride films on amorphous graphene-glass wafer. *Sci. Adv.* **7**, eabf5011 (2021).
44. Chen, Y. et al. Progress and challenges in transfer of large-area graphene films. *Adv. Sci.* **3**, 1500343 (2016).
45. Park, J.-H. et al. Influence of temperature-dependent substrate decomposition on graphene for separable GaN growth. *Adv. Mater. Interfaces* **6**, 1900821 (2019).
46. Amano, H., Sawaki, N., Akasaki, I. & Toyoda, Y. Metalorganic vapor phase epitaxial growth of a high quality GaN film using an AlN buffer layer. *Appl. Phys. Lett.* **48**, 353 (1998).
47. Kawasaki, M. et al. Atomic control of the $SrTiO_3$ crystal surface. *Science* **266**, 1540–1542 (1994).
48. Jiang, J. et al. Carrier lifetime enhancement in halide perovskite via remote epitaxy. *Nat. Commun.* **10**, 4145 (2019).
This paper demonstrates the reduction of dislocations and improvement of optoelectronic properties from remote epitaxy of halide perovskite on NaCl.
49. Shao, Y. et al. Grain boundary dominated ion migration in polycrystalline organic–inorganic halide perovskite films. *Energy Environ. Sci.* **9**, 1752–1759 (2016).
50. Jena, A. K., Kulkarni, A. & Miyasaka, T. Halide perovskite photovoltaics: background, status, and future prospects. *Chem. Rev.* **119**, 3036–3103 (2019).
51. Liu, X. K. et al. Metal halide perovskites for light-emitting diodes. *Nat. Mater.* **20**, 10–21 (2020).
52. Lei, L. et al. Metal halide perovskites for laser applications. *Adv. Funct. Mater.* **31**, 2010144 (2021).
53. Wang, L., King, I., Chen, P., Bates, M. & Lunt, R. R. Epitaxial and quasiepitaxial growth of halide perovskites: new routes to high end optoelectronics. *APL Mater.* **8**, 100904 (2020).
54. Zhou, Z., Qiao, H. W., Hou, Y., Yang, H. G. & Yang, S. Epitaxial halide perovskite-based materials for photoelectric energy conversion. *Energy Environ. Sci.* **14**, 127–157 (2021).
55. Shi, E. & Dou, L. Halide perovskite epitaxial heterostructures. *Acc. Mater. Res.* **1**, 213–224 (2020).
56. Wang, Y. et al. High-temperature ionic epitaxy of halide perovskite thin film and the hidden carrier dynamics. *Adv. Mater.* **29**, 1702643 (2017).
57. Chen, Y. et al. Strain engineering and epitaxial stabilization of halide perovskites. *Nature* **577**, 209–215 (2020).
58. Wang, L. et al. Unlocking the single-domain epitaxy of halide perovskites. *Adv. Mater. Interfaces* **4**, 1701003 (2017).
59. Jeong, J. et al. Remote homoepitaxy of ZnO microrods across graphene layers. *Nanoscale* **10**, 22970–22980 (2018).
60. Jeong, J. et al. Remote heteroepitaxy across graphene: hydrothermal growth of vertical ZnO microrods on graphene-coated GaN substrate. *Appl. Phys. Lett.* **113**, 233103 (2018).
61. Choi, J. et al. Facet-selective morphology-controlled remote epitaxy of ZnO microcrystals via wet chemical synthesis. *Sci. Rep.* **11**, 22697 (2021).
62. Lin, Y. T., Yeh, T. W., Nakajima, Y. & Dapkus, P. D. Catalyst-free GaN nanorods synthesized by selective area growth. *Adv. Funct. Mater.* **24**, 3162–3171 (2014).
63. Li, S. et al. Dependence of N-polar GaN rod morphology on growth parameters during selective area growth by MOVPE. *J. Cryst. Growth* **364**, 149–154 (2013).
64. Jeong, J. et al. Selective-area remote epitaxy of ZnO microrods using multilayer-monolayer-patterned graphene for transferable and flexible device fabrications. *ACS Appl. Nano Mater.* **3**, 8920–8930 (2020).
This paper demonstrates a method to control the position of microstructures in remote epitaxy.
65. Jin, D. K. et al. Position-controlled remote epitaxy of ZnO for mass-transfer of as-deployed semiconductor microarrays. *APL Mater.* **9**, 051102 (2021).
66. Du, D. et al. Epitaxy, exfoliation, and strain-induced magnetism in rippled Heusler membranes. *Nat. Commun.* **12**, 2494 (2021).
67. Koma, A., Sunouchi, K. & Miyajima, T. Fabrication of ultrathin heterostructures with van der Waals epitaxy. *J. Vac. Sci. Technol. B Microelectron. Process. Phenom.* **3**, 724 (1985).
68. Mohseni, P. K. et al. Monolithic III–V nanowire solar cells on graphene via direct van der Waals epitaxy. *Adv. Mater.* **26**, 3755–3760 (2014).
69. Lin, Z., Huang, Y. & Duan, X. Van der Waals thin-film electronics. *Nat. Electron.* **2**, 378–388 (2019).
70. Liu, Y. et al. Van der Waals heterostructures and devices. *Nat. Rev. Mater.* **1**, 16042 (2016).
71. Bae, S. H. et al. Integration of bulk materials with two-dimensional materials for physical coupling and applications. *Nat. Mater.* **18**, 550–560 (2019).
72. Li, X. et al. Transfer of large-area graphene films for high-performance transparent conductive electrodes. *Nano Lett.* **9**, 4359–4363 (2009).
73. Qian, Y. et al. Universal 2D material film transfer using a novel low molecular weight polyvinyl acetate. *Appl. Surf. Sci.* **534**, 147650 (2020).
74. Rang Lim, Y. et al. Resist- and etching-free patterning mediated by predefined photosensitive polyimide for two-dimensional semiconductor-based photodetectors. *Adv. Mater. Interfaces* **8**, 2001817 (2021).
75. Manzo, S. et al. Pinhole-seeded lateral epitaxy and exfoliation on graphene-terminated surfaces. Preprint at https://doi.org/10.48550/arXiv.2106.00721 (2021).
76. Zhao, Z. D. et al. Hydride vapor phase epitaxy of GaN on self-organized patterned graphene masks. *Mater. Lett.* **153**, 152–154 (2015).
77. Lee, J. Y. et al. Multiple epitaxial lateral overgrowth of GaN thin films using a patterned graphene mask by metal organic chemical vapor deposition. *J. Appl. Crystallogr.* **53**, 1502–1508 (2020).
78. Ferrari, A. C. Raman spectroscopy of graphene and graphite: disorder, electron–phonon coupling, doping and nonadiabatic effects. *Solid. State Commun.* **143**, 47–57 (2007).
79. Emery, J. D. et al. Chemically resolved interface structure of epitaxial graphene on SiC(0001). *Phys. Rev. Lett.* **111**, 215501 (2013).
80. Nemes-Incze, P., Osváth, Z., Kamarás, K. & Biró, L. P. Anomalies in thickness measurements of graphene and few layer graphite crystals by tapping mode atomic force microscopy. *Carbon* **46**, 1435–1442 (2008).
81. Takahashi, K., Yamada, K., Kato, H., Hibino, H. & Homma, Y. In situ scanning electron microscopy of graphene growth on polycrystalline Ni substrate. *Surf. Sci.* **606**, 728–732 (2012).
82. Ferrari, A. C. & Basko, D. M. Raman spectroscopy as a versatile tool for studying the properties of graphene. *Nat. Nanotechnol.* **8**, 235–246 (2013).
83. Koh, Y. K., Bae, M. H., Cahill, D. G. & Pop, E. Reliably counting atomic planes of few-layer graphene ($n > 4$). *ACS Nano* **5**, 269–274 (2011).
84. Gass, M. H. et al. Free-standing graphene at atomic resolution. *Nat. Nanotechnol.* **3**, 676–681 (2008).
85. Neubeck, S. et al. Direct determination of the crystallographic orientation of graphene edges by atomic resolution imaging. *Appl. Phys. Lett.* **97**, 053110 (2010).
86. Wang, G. C. & Lu, T. M. *RHEED Transmission Mode and Pole Figures: Thin Film and Nanostructure Texture Analysis* (Springer, 2014).
87. Birkholz, M. *Thin Film Analysis by X-Ray Scattering* (Wiley, 2006).
88. Ul-Hamid, A. *A Beginners' Guide to Scanning Electron Microscopy* (Springer International, 2018).
89. Schwartz, A. J., Kumar, M., Adams, B. L. & Field, D. P. *Electron Backscatter Diffraction in Materials Science* (Springer US, 2009).
90. Giannuzzi, L. A. & Stevie, F. A. *Introduction to Focused Ion Beams: Instrumentation, Theory, Techniques and Practice* (Springer US, 2005).
91. Williams, D. B. & Carter, C. B. *Transmission Electron Microscopy: a Textbook for Materials Science* (Springer US, 2009).
92. Cao, M. C. et al. Theory and practice of electron diffraction from single atoms and extended objects using an EMPAD. *Microscopy* **67**, i150–i161 (2018).
93. Lu, N., Wang, J., Oviedo, J. P., Lian, G. & Kim, M. J. Atomic resolution scanning transmission electron microscopy of two-dimensional layered transition metal dichalcogenides. *Appl. Microsc.* **45**, 225–229 (2015).
94. Huang, P. Y. et al. Grains and grain boundaries in single-layer graphene atomic patchwork quilts. *Nature* **469**, 389–392 (2011).
95. Bae, S. H. et al. Graphene-assisted spontaneous relaxation towards dislocation-free heteroepitaxy. *Nat. Nanotechnol.* **15**, 272–276 (2020).
This paper investigates a spontaneous relaxation mechanism on graphene that can lead to improved material quality in remote heteroepitaxy.
96. Besnard, A., Ardigo, M. R., Imhoff, L. & Jacquet, P. Curvature radius measurement by optical profiler and determination of the residual stress in thin films. *Appl. Surf. Sci.* **487**, 356–361 (2019).
97. Moram, M. A. et al. On the origin of threading dislocations in GaN films. *J. Appl. Phys.* **106**, 073513 (2009).
98. Si, M. et al. A ferroelectric semiconductor field-effect transistor. *Nat. Electron.* **2**, 580–586 (2019).
99. Salahuddin, S. & Datta, S. Use of negative capacitance to provide voltage amplification for low power nanoscale devices. *Nano Lett.* **8**, 405–410 (2008).
100. Abel, S. et al. Large Pockels effect in micro- and nanostructured barium titanate integrated on silicon. *Nat. Mater.* **18**, 42–47 (2018).
101. Garcíа De Arquer, F. P., Armin, A., Meredith, P. & Sargent, E. H. Solution-processed semiconductors for next-generation photodetectors. *Nat. Rev. Mater.* **2**, 16100 (2017).
102. Yu, W. et al. Single crystal hybrid perovskite field-effect transistors. *Nat. Commun.* **9**, 5354 (2018).
103. Shi, J. A structurally unstable semiconductor stabilized and enhanced by strain. *Nature* **577**, 171–172 (2020).
104. Li, J., Shan, Z. & Ma, E. Elastic strain engineering for unprecedented materials properties. *MRS Bull.* **39**, 108–114 (2014).

105. Cao, A. et al. Design and fabrication of an artificial compound eye for multi-spectral imaging. *Micromachines* **10**, 208 (2019).
106. Tang, X., Ackerman, M. M., Chen, M. & Guyot-Sionnest, P. Dual-band infrared imaging using stacked colloidal quantum dot photodiodes. *Nat. Photonics* **13**, 277–282 (2019).
107. Zou, Y. et al. in *Proc. SPIE 11703, AI and Optical Data Sciences II* Vol. 11703 (eds Jalali, B. & Kitayama, K.) 127–132 (SPIE, 2021).
108. Ma, J., Yu, W., Liang, P., Li, C. & Jiang, J. FusionGAN: a generative adversarial network for infrared and visible image fusion. *Inf. Fusion* **48**, 11–26 (2019).
109. Yao, P. et al. Fully hardware-implemented memristor convolutional neural network. *Nature* **577**, 641–646 (2020).
110. Woźniak, S., Pantazi, A., Bohnstingl, T. & Eleftheriou, E. Deep learning incorporating biologically inspired neural dynamics and in-memory computing. *Nat. Mach. Intell.* **2**, 325–336 (2020).
111. Wang, Z. et al. Resistive switching materials for information processing. *Nat. Rev. Mater.* **5**, 173–195 (2020).
112. Kaspar, C., Ravoo, B. J., van der Wiel, W. G., Wegner, S. V. & Pernice, W. H. P. The rise of intelligent matter. *Nature* **594**, 345–355 (2021).
113. Gu, L. et al. A biomimetic eye with a hemispherical perovskite nanowire array retina. *Nature* **581**, 278–282 (2020).
114. Rao, Z. et al. Curvy, shape-adaptive imagers based on printed optoelectronic pixels with a kirigami design. *Nat. Electron.* **4**, 513–521 (2021).
115. Yeon, H. et al. Long-term reliable physical health monitoring by sweat pore-inspired perforated electronic skins. *Sci. Adv.* **7**, eabg8459 (2021).
116. Ryu, H., Wu, H., Rao, F. & Zhu, W. Ferroelectric tunneling junctions based on aluminum oxide/zirconium-doped hafnium oxide for neuromorphic computing. *Sci. Rep.* **9**, 20383 (2019).
117. Huang, J.-L. et al. in *Proc. 2017 IEEE 30th International Conference on Micro Electro Mechanical Systems (MEMS)* 1188–1191 (Institute of Electrical and Electronics Engineers, 2017).
118. Guo, Z. et al. Self-powered sound detection and recognition sensors based on flexible polyvinylidene fluoride–trifluoroethylene films enhanced by in-situ polarization. *Sens. Actuators A Phys.* **306**, 111970 (2020).
119. Deng, J. et al. A tactile sensing textile with bending-independent pressure perception and spatial acuity. *Carbon* **149**, 63–70 (2019).
120. Zhang, Z., Tian, Z., Mei, Y. & Di, Z. Shaping and structuring 2D materials via kirigami and origami. *Mater. Sci. Eng. R Rep.* **145**, 100621 (2021).
121. Wang, W. et al. Kirigami/origami-based soft deployable reflector for optical beam steering. *Adv. Funct. Mater.* **27**, 1604214 (2017).
122. Otoole, M., Lindell, D. B. & Wetzstein, G. Confocal non-line-of-sight imaging based on the light-cone transform. *Nature* **555**, 338–341 (2018).
123. Alaskar, Y. et al. Towards van der Waals epitaxial growth of GaAs on Si using a graphene buffer layer. *Adv. Funct. Mater.* **24**, 6629–6638 (2014).
124. Anyebe, E. A. & Kesaria, M. Recent advances in the Van der Waals epitaxy growth of III–V semiconductor nanowires on graphene. *Nano Select* **2**, 688–711 (2021).
125. Khan, A. et al. Direct CVD growth of graphene on technologically important dielectric and semiconducting substrates. *Adv. Sci.* **5**, 1800050 (2018).
126. Zhang, Y. et al. Capillary transfer of soft films. *Proc. Natl Acad. Sci. USA* **117**, 5210–5216 (2020).
127. Song, S. W. et al. Direct 2D-to-3D transformation of pen drawings. *Sci. Adv.* **7**, eabf3804 (2021).
128. Yu, J. et al. Van der Waals coherent epitaxy of GaN and InGaN/GaN multi-quantum-well via a graphene inserted layer. *Opt. Mater. Express* **11**, 4118–4129 (2021).
129. Badokas, K. et al. Remote epitaxy of GaN via graphene on GaN/sapphire templates. *J. Phys. D Appl. Phys.* **54**, 205103 (2021).
130. Chang, J.-H. et al. MOVPE growth of GaN via graphene layers on GaN/sapphire templates. *Nanomaterials* **12**, 785 (2022).
131. Guo, Y. et al. A reconfigurable remotely epitaxial VO_2 electrical heterostructure. *Nano Lett.* **20**, 33–42 (2020).
132. Jia, R. et al. Van der Waals epitaxy and remote epitaxy of $LiNbO_3$ thin films by pulsed laser deposition. *J. Vac. Sci. Technol. A Vac. Surf. Films* **39**, 040405 (2021).
133. Lu, Z. et al. Remote epitaxy of copper on sapphire through monolayer graphene buffer. *Nanotechnology* **29**, 445702 (2018).
134. Wang, D. et al. Remote heteroepitaxy of atomic layered hafnium disulfide on sapphire through hexagonal boron nitride. *Nanoscale* **11**, 9310–9318 (2019).
135. Chae, S. et al. Lattice transparency of graphene. *Nano Lett.* **17**, 1711–1718 (2017).
136. Kim, Y. et al. Fabrication of a microcavity prepared by remote epitaxy over monolayer molybdenum disulfide. *ACS Nano* **16**, 2399–2406 (2022).
137. Franchi, S., Trevisi, G., Seravalli, L. & Frigeri, P. Quantum dot nanostructures and molecular beam epitaxy. *Prog. Cryst. Growth Charact. Mater.* **47**, 166–195 (2003).
138. Nakamura, F., Kim, Y. D., Yoon, E., Forbes, D. V. & Coleman, J. J. Thickness monitoring of GaAs growth by surface photoabsorption in metalorganic chemical vapor deposition. *J. Appl. Phys.* **83**, 775–778 (1998).
139. Gatzen, H. H., Saile, V. & Leuthold, J. in *Micro and Nano Fabrication* Ch. 6, 313–395 (Springer, 2015).
140. Ferrari, A. C. et al. Raman spectrum of graphene and graphene layers. *Phys. Rev. Lett.* **97**, 187401 (2006).

Acknowledgements
This work is supported by the Defense Advanced Research Projects Agency Young Faculty Award (award no. 029584-00001), the US Department of Energy's Office of Energy Efficiency and Renewable Energy (EERE) under the Solar Energy Technologies Office (award no. DE-EE0008558) and the Air Force Research Laboratory (no. FA9453-21-C-0717). H.S.K. acknowledges support by Yonsei University Research Fund of 2021-22-0338. Y.J.H. and J. Jeong acknowledge support by the National Research Foundation (NRF) of South Korea (NRF-2021R1A5A1032996; 2020R1F1A1074477).

Author contributions
Introduction (H.K. and J.K.); Experimentation (all authors); Results (C.S.C., S.L., J. Jiang and J.S.); Applications (all authors); Reproducibility and data deposition (Y.M. and S.-H.B.); Limitations and optimizations (M.P., K.L., J. Ji, Y.K. and H.S.K.); Outlook (H.K. and J.K.); Overview of the Primer (all authors).

Competing interests
The authors declare no competing interests.

Peer review information
Nature Reviews Methods Primers thanks Zhaolong Chen and the other, anonymous, reviewer(s) for their contribution to the peer review of this work.

Publisher's note
Springer Nature remains neutral with regard to jurisdictional claims in published maps and institutional affiliations.

Supplementary information
The online version contains supplementary material available at https://doi.org/10.1038/s43586-022-00122-w.